Improved Accuracy for Indoor Positioning with Bluetooth 5.1: From Theory to Measurements

Victor Sesma and Victor Egorov
sesmavictor@yahoo.es - victoras.egorov@gmail.com

Department of Electrical and Information Technology
Lund University

Supervisor: Harsh Tataria - Peter Karlsson

Examiner: Fredrik Rusek

September 1, 2020

Printed in Sweden
Tryckeriet i E-huset, Lund

Abstract

In this thesis we are evaluating Bluetooth Low Energy (BLE) v5.1 in combination with Direction Of Arrival (DOA) algorithms and receiving antenna arrays for indoor positioning systems. The thesis is divided in two parts. The first part is the core of the thesis and is composed by the evaluation of DOA algorithms in a direction finding system. A campaign of measurements is carried out in an active indoor human environment. We aim for a suitable antenna configuration and DOA algorithm that will result in an angular error estimation below 10°. In the process, we evaluate the implications of the frequency in AOA estimation and we propose an algorithm that is based on frequency diversity in order to make angular estimation errors more robust. The objective is successfully complied using a 4x4 URA receiver together with PDDA DOA estimation algorithm reaching a Mean Absolute Error (MAE) of 4.15°. The second part of the thesis consists of demonstrating that a sub-meter error accuracy is possible using Bluetooth v5.1. To do so, we use the findings from the first part of the thesis and we present a simple geometric approach to estimate the position of the transmitter. The positioning engine is based on AOA and RSSI parameters. The objective is again successfully completed, obtaining an average distance error of 0.88 m.

Keywords: Indoor Positioning, BLE, DOA algorithms, PDDA, MAE, RSSI

Popular Science Summary

A hot topic of the last decade is the smart devices that can "talk" to each other. From a time where internet was used to connect people across the world, we have arrived at an Era where it connects devices that communicate without human interference. This connectivity of the devices to the network and the exchange of the data is referred as the Internet of Things (IoT).
Ericsson made a prediction that, by the year 2025, the IoT devices that will be connected to the network will surpass the global population over three times reaching the astonishing number of more than 24.9 billion connections [44].
The expectation is that an increasing number of items connected to the internet will do additional tasks. Smartphones, vehicles, and countless gadgets use GPS system for navigation, tracking and positioning. GPS has proved to be a reliable and accurate radio-navigation system which enhanced connectivity and global mapping. However, using GPS for indoor purposes remains a challenge as propagating through walls and levels of floors is still an obstacle, as the signal is heavily deteriorated. Indoor positioning systems can take advantage of that. Using communication technologies such as Bluetooth, indoor environments can be mapped. Thus, indoor tracking, navigation and positioning accuracy are increased resulting to higher precision. This concept can be applied in various aspects of society, like health care, transportation, entertainment or safety measurements.
People who are running late with their flight will not lose time as they will be guided directly to their gate. In museums, information provided to peoples headphones will be changed accordingly to where they stand and what they observe. Patients in hospitals will have increased supervision, enabling prioritisation of the patients by the caregivers. Managers will be able to use the information from the data gathered to provide a more efficient and pleasant environment for their employees. There are numerous aspects in the society and services that can profit from indoor positioning systems.
We do indoor positioning measurements in an office environment using Bluetooth v5.1 as a communication technology. This version of Bluetooth holds information about the direction of the incoming source. We use this information in combination with appropriate algorithms that provide the angles of the source and received signal strength indicator (RSSI). Through that we strive to reach an increased precision of indoor positioning.

Acknowledgements

Firstly, we would like to thank Lund University for giving us the opportunity to study in a top international high education institution. We received an outstanding education in the Wireless Communication Master's programme.
We would like to thank Peter Karlsson, our supervisor from ublox company, for this opportunity. For the interesting project provided, the helpful advice and guidance across the thesis project, and for making us feel like we are part of the ublox community.
We would like to thank Harsh Tataria, our supervisor from Lund University, for the perceptive discussions, the constructive feedback, and the guidance that he provided us.
Lastly, we would like to thank Andreas Karlqvist, Mohamad Abou Nasa and Farshid Rezaei, ublox employees, for all the assistance, discussions, and welcoming atmosphere that they provided.
You truly made this thesis a pleasant and enriching experience for us. Thank you all.

Table of Contents

List of Figures

List of Tables

Chapter 1
Introduction

1.1 Background and Motivation

In the last decade we have had an exponential increase in smart phones and wireless devices that has resulted in a wide range of applications and services. A service that has gained huge interest is the ability to track and locate the position of the devices [1]. The position information of any individual device is fundamental for the user for daily applications involving navigation, object localization and guidance. In outdoor scenarios, the widely used Global Positioning System (GPS) is an effective technology used for positioning purposes. GPS is known to provide from tens of meters to sub-meter of positioning accuracy relative to the ground truth [2]. The signal that is coming from the satellites is affected by multipath, fading, and blockage if there are high buildings. Additionally, when that signal is penetrating into indoor environments, the position accuracy of GPS significantly decreases. This is due to the combination of signal strength attenuation and interference from other Ultra High Frequency (UHF) band services, such as mobile phones, Bluetooth, ZigBee, satellite radio, remote control systems, and television broadcast among others. An indoor measurements campaign evaluating GPS for indoor positioning performance has shown that the signal power of most of the satellites has a range of -140 to -160 dBm [3], while a typical signal power from a GPS satellite is -125 dBm [7]. They have concluded that using indoor traditional receivers gave deceitful results which led to position estimations that were inaccurate [3].

To this end, the pursuit for indoor positioning began as the majority of wireless data traffic is taking place indoors and hence it is of paramount importance to localize indoor users. Viewing it from the market perspective, the Indoor Positioning Systems (IPS) can give insight on how people are moving around. These insights can provide knowledge on how an area with a lot of human traffic can improve to make the environment dynamically adaptive, ergonomic, and friendlier for the people. IPS will give rise to a great number of other applications as well. These applications can provide utilities that can enhance the experience of the users. People working in warehouses will save time in search of goods as they can have knowledge, in real time, of their exact position. Guidance can be provided to visually impaired people through difficult indoor scenarios such as airports or malls. A myriad of companies [5], app developers [6], and the research commu-

nity itself [1] have shown interest in IPS as a result. Consequently, much research has been carried out in the indoor localization and positioning area using different technologies such as WiFi, Bluetooth, Radio Frequency Identification (RFID), ZigBee, and Ultra-Wide Band (UWB) systems among many others. Important parameters that are considered is the power consumption [10] and the cost. The applications that enable localization are an additional service for the end user device. IPS that are not energy efficient and consume the devices' battery need to be avoided. The latest version of Bluetooth, also known as Bluetooth Low Energy (BLE) v5.1 adds to the well known existing low consumption features, an enhanced direction finding feature which makes it a promising technology for IPS applications [13]. BLE v5.1, is a wireless standard used in short-range communications. Two of its features are that it can provide a coverage up to 100 m [14] and has power consumption lower than its previous versions, which makes it an appropriate technology for indoor scenarios. By 2021 ABI Research predicts there will be 48 billion devices connected to the internet and 30% of those are predicted to include Bluetooth technology [15]. The connection of different things to the internet, commonly referred to as Internet of Things (IoT), is very attractive for IPS, and Bluetooth will be a key enabler[15]. IoT will not only play a prominent part in IPS but will have a key role in the deployment of the fifth generation (5G) where 5G mm-wave communications systems can be used to achieve high accuracy in indoor localization [16]. As can be seen, indoor positioning will be one of the factors that will contribute to a world where people, data, processes, and things will be brought together, referred to as the Internet of Everything (IoE) [17].

1.2 Purpose and Aims of the Thesis

The objective of this thesis is to evaluate the newest Bluetooth v5.1 wireless standard in indoor environments for an enhanced positioning system. Bluetooth v5.1 is promising for indoor position estimation in comparison to the early standards because it adds Direction Of Arrival (DOA) features which enables it to estimate the Angle of Arrival (AOA) and Angle of Departure (AOD). The number of antenna elements and array configurations fundamentally limit the DOA accuracy, since the angular resolution of the array (Rayleigh resolution) directly scales linearly with the number of antennas. Thus, evaluation will be done on different antenna configurations and angular estimation will be calculated based on different AOA estimation algorithms. The AOA algorithms that will be considered are PDDA, MUSIC, SSS, and ESPRIT. In order to decrease hardware and computational effort, which leads to faster response in real time estimations, we aim to do an evaluation based on some parameters. These parameters will be the antenna elements, number of BLE packets, number of snapshots, angular step size of the steering vector and the elapsed time of each AOA algorithm considered above. **The objective of this thesis is to come to an optimal combination of antenna array configuration, and an enhanced AOA estimation algorithm that results in an angular error below 10 degrees**. In consideration of the aims mentioned above, a virtual positioning system with four anchors is proposed in order to demonstrate and implement the proposed algorithm in a real

and varying indoor environment where the robustness of the algorithm is analysed.

1.3 Methodology

The core of this project relies on antenna measurements and signal processing. In order to obtain angular estimations, first a measurement campaign is done in two different scenarios; direction finding measurement and virtual positioning measurement. This implies a complete knowledge of the hardware in use, such as, antennas, modules, controllers and computers. The scenario where the measurements are taken is also analyzed in terms of distances and materials in order to have an expectation of the final results regarding angular estimations. The transition from measurements to signal processing is being carried out meticulously. First, short tests are done in order to check that the system is working as expected, that means a pre-analysis of the data, consisting of an examination of the IQ samples' quality. This process will be expanded in later chapters. The verification is carried out before a full measurement corresponding to one receiving antenna array. The measurements are performed using internal software. From the modules perspective, a C code is used when it comes to flashing and pin connections allocation. From the hardware perspective, a Python code is used to set up parameters that involves the data acquisition and it is also in charge of controlling mechanically the antennas. Once the set of data is acquired, the signal processing is carried out in MATLAB, where the analysis of the measurements using AOA estimation algorithms takes place. Finally, a final measurement with four virtual anchors, in a dynamic office environment, is done following the previous process.

1.4 Literature Review

Indoor positioning has resulted to be a hot topic. Since the introduction of BLE [18] numerous research has been conducted on positioning [24], [25] with very promising results. With BLE, the Bluetooth beacon [19] came to the market. Beacon is used to transmit data in a specific distance range. Devices that are located within its distance range pick up the signal. This provides information related to the beacons' surrounding. The limitation of this application, from the perspective of position estimation, is that the end user device has no other information about the beacon besides the Received Signal Strength Indicator (RSSI). This implies that the distance can be estimated but the position of the beacon itself cannot be located. Furthermore, the dispersion of the advertising channel of the beacon generates different RSSI, which results in a moderate accuracy of the position [26].
To estimate the position of the beacon in [20], they use an AOA estimation algorithm known as MUltiple SIgnal Classification (MUSIC), and two anchors with known position. With this approach they show that the the position of the beacon can be estimated in a predefined indoor environment with an average accuracy of 14 cm. The problem of positioning using this method remains, as it requires extra hardware and anchors with multiple elements under a supervised environment to achieve that accuracy. This means that solutions need to be proposed,

fitting the existing hardware of the end user device or the wireless standard. A solution comes from the latter as BLE adds directional finding features in the new standard v5.1 [13]. Researchers at the University of Edinburgh published a paper about BLE v5.1 and the positioning system [4]. In their empirical evaluation they concluded that the localization range is constrained and the positioning is in sub-meter accuracy. Nonetheless, at the time of their experiment with BLE v5.1 there were still no hardware available at the market with these features. Thus, they used a Software Defined Radio (SDR) to imitate the transmission and reception of BLE with the AOA method. However, extensive research needs to be done under different environments with different antennas to acquire more information about angular accuracy and estimation.

1.5 Thesis Organization

This thesis is organized into five chapters. In the first chapter, Introduction, we describe the reasons for carrying out this thesis and our aims under certain limitations. The second chapter, Theoretical Background, is a summary of the theory that is used in this thesis. The third chapter, Bluetooth v5.1 Direction Finding, is where the campaign of measurements for AOA estimation is taking place and the algorithm for AOA estimation is proposed. The fourth chapter, Bluetooth v5.1 Position Finding, is where the campaign of measurements for position estimation is conducted and the position finding is based on the proposed AOA algorithm and the RSSI. Concluding with chapter five, where we discuss our conclusions and possible future research that can further enhance the performance of the indoor positioning estimations.

1.6 Limitations

In chapter four, after doing some measurements to acquire RSSI data, we noticed instabilities in the level of RSSI which made hard to extract a Path-Loss model. Hence, we assume knowledge of the Path-Loss. Thus for the positioning estimation, the distance between the transmitter and the receiver is known.

Chapter 2
Theoretical Background

2.1 Introduction to BLE v5.1

Bluetooth technology has experienced a significant evolution over the past two decades where it started in 1998 as Bluetooth Special Interest Group (SIG) [8]. It has had a great impact in technology, having expanded worldwide, and having been implemented in a large variety of devices such as mobile phones, computers, headphones, speakers, and smartphones [8].
Bluetooth SIG has deployed several versions of Bluetooth over the past years adding new features and improving the capabilities of this wireless technology. The first mobile phone with Bluetooth capabilities was launched in 2000 and it was not until 2004 that this technology became widespread [8]. In 2004, Bluetooth 2.0 was implemented with Enhanced Data Rate (EDR) technology, reaching data rates of 3 Mbit/s [8]. The evolution of the next versions relied on the improvement of the data rate, security features, positioning, low energy and range, Bluetooth 5.0 being its maximum exponent. This evolution comes together with the increase of connected wireless devices (IoT). Figure 2.1 depicts the shipment increment of devices with Bluetooth.

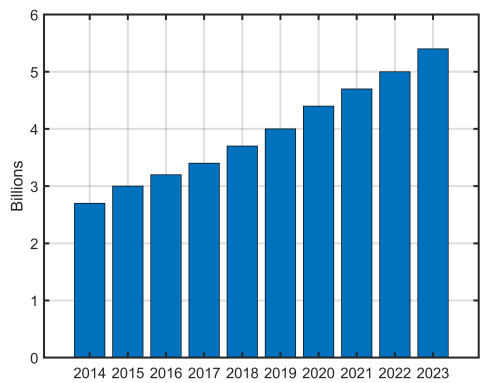

Figure 2.1: Annual Bluetooth device shipments [9] .

The launching of BLE in 2010 [18] granted the ability to companies to produce low cost, energy efficient, real time locating systems and indoor positioning systems besides others. Bluetooth categorized these localization systems based on the proximity and based on the position. In the proximity fall services that calculate the in between distance of two devices. Examples are Point of Interest (PoI) information and item finding using Bluetooth tags [36]. In the position fall services that are locating items in real time and indoor positioning systems. In both cases the information of the position is known based on the RSSI and the reference signal strength by applying geometric calculations. Indoor positioning systems' as well as real time location systems' positioning accuracy is affected by different factors like environmental conditions and dense human trafficking. Thus, the position accuracy can be given in the meter level [36]. This gives rise to obstacles as there are systems that require accuracy in positioning in sub-meter level.

In 2019, Bluetooth SIG released the newest Bluetooth Low Energy (BLE) v5.1 version. The main addition of this version relies on enhanced positioning capabilities [11]. In previous versions, the positioning was mainly based on the received signal power information (RSSI), which leads to non entirely accurate positioning on indoor environments. This is greatly improved in BLE v5.1, where DOA features are implemented to help improving the positioning accuracy [11]. BLE v5.1 protocol and DOA features are expanded in later chapters.

2.2 Introduction to Multiple Antenna Systems

In the late 1880s, Markov and Popov among others designed the first original antenna. A few years later in 1900s Marconi developed directional antennas for his proposed cross-Atlantic links and in the twentieth century, antenna design improved in terms of frequency of operation and bandwidth. One of the important findings was the Yagi-Uda array which offered high bandwidth and gain. In 1950s the patch antenna was developed offering low profile and cost. The use of antennas in array form was first implemented in World War II essentially for radar applications. As an example, Wullenweber arrays were designed in 1938 operating at low frequencies and focusing on the accuracy, which is still used in nowadays aircraft localization systems [12].

Wireless communication technology is rapidly changing the past few years. The huge number of users connected in the same space and time makes it challenging for wireless system designers to adopt a robust and efficient technology to this end [12]. The reason behind this challenge relies on the limited radio frequency spectrum resource, a complex time-varying wireless environment, the necessity of higher data rates, better Quality of Service (QoS) and so on. Multiple antenna system is a technology that provides promising improvements facing these limitations [12]. Apart from the mentioned link performance parameters, Multiple Antenna System plays a key role also in positioning. This role will be exposed in next chapters evaluating the benefits and theory behind Multiple Antenna Systems in positioning techniques.

2.3 Direction Estimation Parameters

In this thesis, the technique used to estimate the direction of the source is the AOA technique. This method simply consists of estimating the incoming angular direction of the electromagnetic wave excited by the source. The process is based on analyzing the received waves' phase difference between the antenna elements. As the source is located in a three dimensional space, it is important to introduce the spherical coordinate system [27] and notation that will be followed for the angular estimation. As it can be seen from Figure 2.2, the azimuth angle corresponds to ϕ, while the elevation angle corresponds to θ. The distance between the receiver and the source is denoted by r.

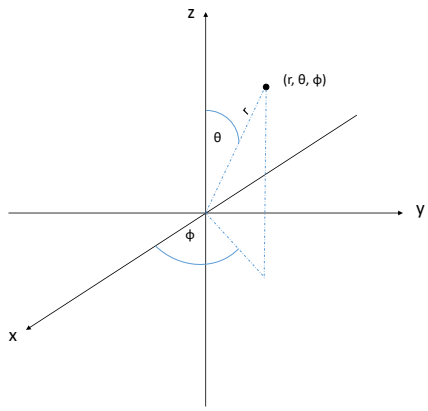

Figure 2.2: Set of Spherical Coordinates.

Conversion from spherical to cartesian coordinates [27] will facilitate future derivations regarding signal models. The cartesian coordinates are defined as,

$$\begin{cases} x = d_x \sin\theta \cos\phi \\ y = d_y \sin\theta \sin\phi \\ z = d_z \cos\theta \end{cases}, \tag{2.1}$$

The direction estimation is based on a peak detection in the angular spectrum, which is given by the AOA estimation algorithms. These algorithms do not provide the received real power spectrum but a reconstruction of it. Thus, we refer to these spectrums as pseudo-spectrums. Depending on the approach used, we can have a two-dimensional or a three-dimensional pseudo-spectrum. In a two-dimensional pseudo-spectrum (Figure 2.3a) we are only resolving power from one plane, azimuth or elevation plane. On the other hand, in a three-dimensional pseudo-spectrum (Figure 2.3b) the power is resolved in both the azimuth and elevation planes. The power of the pseudo-spectrums will be normalized to help visualizing possible differences between the main lobe and other secondary lobes.

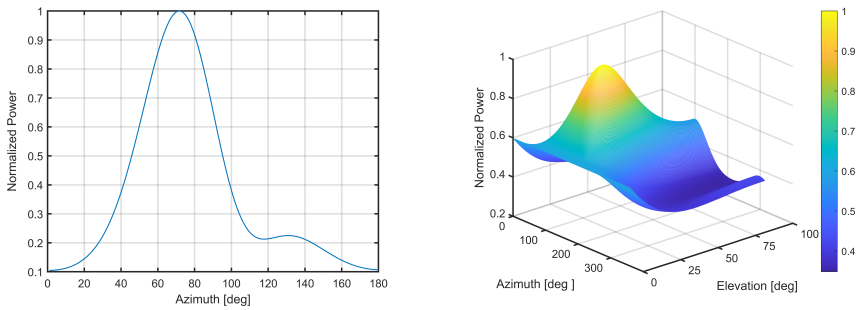

(a) Two-dimensional Pseudo-spectrum **(b)** 3D Pseudo-spectrum

Figure 2.3: Angular Pseudo-spectrum

2.4 Received Signal Model

The following section explains the mathematical model for the array and incoming signals. It is important to introduce this theory since the AOA estimation is based on the phase difference between elements of an array. First, the Uniform Linear Array (ULA) is exposed for the reason that this type of array is giving a clear picture of the physical interpretation of the received signal model. Having settled the basis of ULA, the theory is expanded to Uniform Rectangular Arrays (URA) since the experiments are carried out with this type of array.

It is important to state that as we are using BLE v5.1 in the ISM band with 20 MHz of channel bandwidth, the signal is narrowband in the RF sense, i.e, the bandwidth of the signal is much smaller than the carrier frequency ($BW_{signal} << f_c$). Thus, we consider frequency-flat channels with the same response. However, although we are in the narrowband condition, this does not imply that the corresponding bandwidth of BLE is frequency flat, it can be frequency selective [12] between adjacent channels as it is discussed later in this thesis.

Another aspect to be mentioned is that the source is located in the far field respect to the receiving antenna, which eliminates the non-linearities that occur in the near field and considers a received planar wavefront in order to extract the phase needed for AOA estimation.

2.4.1 Uniform Linear Array (ULA)

In this case (Figure 2.4), the configuration consists of M elements linearly and uniformly placed on the same plane separated by d_x distance. The directional angle ϕ arriving at the array is known as Direction of Arrival (DOA) [21]. In this thesis we only contemplate one source, so the following exposed received signal model considers only one source. If more than one source needs to be taken into consideration, this model can be expanded straightforward.

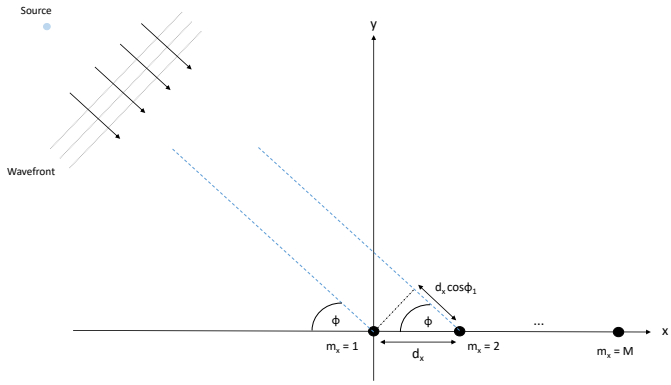

Figure 2.4: Horizontal plane waves incident on ULA.

Let's define r_m(t) as the signal received at the m-th element, s(t) as the incident signal coming from the source and n_m(t) the additive white gaussian noise (AWGN) at the m-th element. The relationship between the transmitted signal and the received signal at the m-th antenna element is defined as,

$$r_m(t) = a_m s(t - \tau_m) + n_m(t), \tag{2.2}$$

where τ_m is the propagation delay between the transmitter and the m-th antenna element and a_m is the complex amplitude of the received signal at the m-th element. The fact that the antennas are separated by d_x distance leads to a phase shift since there is a difference in propagation delay between elements [21]. Using the space, time and speed relationship, the time of arrival difference between the first two elements is given by,

$$\tau_2 - \tau_1 = (d_x/c_0)\cos(\phi), \tag{2.3}$$

Thus, the expression for the received signal at the second antenna element is the following,

$$r_2(t) = a_2 s(t - \tau_1) e^{-j2\pi d_x \cos(\phi)/\lambda_0} + n_2(t), \tag{2.4}$$

The received signal expression for the rest elements is obtained by replacing the delay equation given in (2.3) into the general equation (2.2). Joining all the received signals equations from each element we obtain a general expression of the following form,

$$\mathbf{r}(t) = \mathbf{a}(\phi)\mathbf{s}(t) + \mathbf{n}(t), \tag{2.5}$$

where $\mathbf{r}$(t) is a MxK vector, $\mathbf{s}$(t) is a 1xK vector and $\mathbf{n}$(t) is a MxK vector. K corresponds to the total number of snapshots, i.e, time instances. $\mathbf{a}(\phi)$ is the steering vector, Mx1 dimension, which follows the classical Vandermonde structure given by,

$$\mathbf{a}(\phi) = \begin{bmatrix} 1 \\ e^{-jk_0 d_x \cos(\phi)} \\ e^{-jk_0 2d_x \cos(\phi)} \\ \vdots \\ e^{-jk_0 (M-1) d_x \cos(\phi)} \end{bmatrix}, \tag{2.6}$$

According to (2.6) we can define the steering vector in a general form. In this form we consider resolution in both planes, so the equation is the following,

$$\mathbf{a}(\phi, \theta) = \begin{bmatrix} e^{-jk_0 s_1} \\ e^{-jk_0 s_2} \\ \vdots \\ e^{-jk_0 s_M} \end{bmatrix}, \tag{2.7}$$

where s_{m} is the physical position according to cartesian coordinates (2.1) of the m-th element.
Thus, it is clear that the use of ULA configuration limits the AOA estimation to only two dimensions. However, as it shown in the next sections, the use of URAs permits to extend the AOA estimation capabilities to three dimensions. The general equation of the model (2.5) remains valid for URA configurations except for the steering vector which varies depending on the geometry of the array. In the next section the steering matrix of URAs is introduced.

2.4.2 Uniform Rectangular Array (URA)

We can see the uniform rectangular array configuration as multiple uniform linear arrays. In AOA terms, the consequence of this configuration relies on the possibility of resolving power from both azimuth and elevation. Thus, using the general equation (2.5) we can characterize the received signal model for URAs.
As the geometry of URAs differs from UCAs and ULAs, the steering matrix $\mathbf{A}(\theta,\phi)$ will be different.

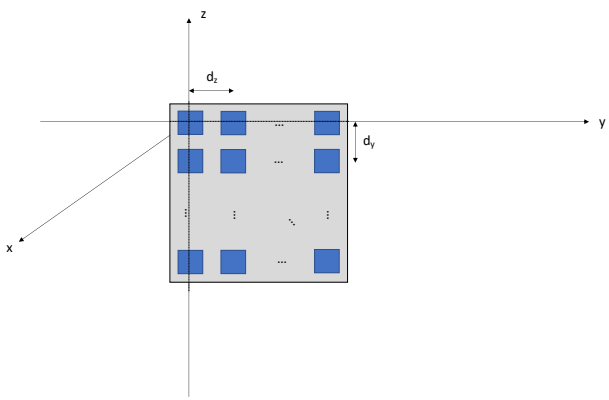

Figure 2.5: URA configuration.

Figure 2.5 shows the MxN URA geometry placed on the vertical z-y plane. The reason for this orientation is that the measurements are been carried out looking for angular resolutions in the frontal plane. The vertical and horizontal elements separation is denoted by d_z and d_y respectively.
Using (2.1), the position of the elements is obtained and we can deduce the steering matrix for the URA. We denote m and n as the m-th and n-th element in the y and z planes respectively. So, using (2.7) we find the entries of the steering vector for URA given by,

$$\mathbf{a}_{mn}(\theta, \phi) = e^{jk_0(md_y \sin\theta \sin\phi + nd_z \cos\theta)}, \tag{2.8}$$

The URA configuration influences the distribution of the azimuth and elevation angles. We assume that the elements consist of patches, thus, they can only receive energy from the frontal plane. The angular distribution with this orientation is,

$$-\pi/2 \leq \phi \leq \pi/2, \tag{2.9}$$

$$0 \leq \theta \leq \pi, \tag{2.10}$$

2.5 Direction of Arrival (DOA) Estimation Algorithms

A large variety of methods have been proposed in literature on DOA estimations. This estimations refers to the process of retrieving the direction information of one or several sources from the output of the receiving antenna array. Thus, these estimations are based on the signal angular spectrum since the signal is distributed on every direction of the space. The array structure of the receiver provides spatial sampling of this waveform.
Much research has been conducted on array signal processing to estimate the DOA through different efficient direction finding techniques. These methods can be divided in AOA and AOD methods. This is happening by exploiting the structure of array and the Time Difference Of Arrival (TDOA) of the signal. Under narrowband and far-field conditions, the wave of the signal is taken as a plane-wave. When it arrives at the array, there will be a TDOA between different elements. This time difference is translated into a phase difference that each element has with its consecutive element. In that way the incoming direction of the signal is estimated.
These methods can be grouped as spectral based methods like MUSIC [29], Capon [30], Barlett beam-former (BF) or parametric based like Maximum Likelihood (ML) [31]. These methods give different performances according to computational effort, robustness and accuracy. DOA estimation accuracy can be affected by many factors such as Signal to Noise Ratio (SNR), sampling period, physical phenomena like reflection, refraction and diffraction among many others.
The algorithms that will be used for AOA estimation are based on spectral based methods; Multiple Signal Classification (MUSIC), Propagator Direct Data Acquisition (PPDA) [32], and Subtracting Signal Subspace (SSS) method [33]. All

these algorithms are characterized by high angular resolution and sensitivity. Another algorithm that will be evaluated is the Estimation of Signal Parameters via Rotational Invariance Technique (ESPRIT) due to its low complexity [34].

2.5.1 Propagator Direct Data Acquisition (PDDA)

PDDA is a low complexity method. The main difference compared with MUSIC and SSS is that it is not necessary to compute the correlation matrix of the received signal nor the eigenvalue decomposition. This results in a significant decrease in computational effort.
Hypothesize, that the received MxK data matrix $\boldsymbol{r}(t)$, has K snapshots of data received from M elements. First, the $\boldsymbol{r}(t)$ matrix is divided into two sub-matrices, $\boldsymbol{h}$ (2.18) and $\boldsymbol{H}$ (2.19). The former is a 1xK vector containing the first row of $\boldsymbol{r}(t)$ and the later is a M-1 x K matrix.

$$\boldsymbol{h} = [r_1(t_1)\ r_1(t_2)\ \ldots\ \ldots\ r_1(t_K)], \tag{2.11}$$

$$\boldsymbol{H} = \begin{bmatrix} r_2(t_1)\ r_2(t_2) & \cdots & \cdots & r_2(t_K) \\ \vdots\ \vdots & \ddots & \vdots & \vdots \\ \vdots\ \vdots & \vdots & \ddots & \vdots \\ r_M(t_1)\ r_M(t_2) & \cdots & \cdots & r_M(t_K) \end{bmatrix}, \tag{2.12}$$

Then, the 1xM-1 propagator vector, i.e, the cross-correlation between the received signal of the first element and the rest is defined (2.20). This vector contains the information of how the signals' phasors are changing over the array and it is represented as a summation of the phases at each element. This operation leads to a normalization of the first elements phases which leads to independency on the signal time series, enhancing the robustness to noise [5]. Thereupon, with one or few snapshots, the AOA can be estimated efficiently without the need of prior knowledge of the number of sources, even when they are greatly correlated.

$$\boldsymbol{p} = \frac{\boldsymbol{h}\boldsymbol{H}^H}{\boldsymbol{h}\boldsymbol{h}^H}, \tag{2.13}$$

We now construct the 1xM $\boldsymbol{e}$ vector, by adding a unit element, which represents the correlation of the first row with itself as shown by,

$$\boldsymbol{e} = [1\ \boldsymbol{p}]^T, \tag{2.14}$$

Finally, the angular pseudo-spectrum according to PDDA algorithm is defined as,

$$P_{PDDA}(\phi, \theta) = |\boldsymbol{A}(\phi, \theta)^H \boldsymbol{e}|^2, \tag{2.15}$$

The following table (Table 2.3) and figure (Figure 2.9) show an example of PDDA algorithm code and pseudo-spectrum.

PDDA Algorithm

```
function [Ppdda] = PDDA (M, elevation_range, azimuth_range, A, Received_signal)

h = Received_signal( 1 , : );

H = Received_signal ( 2:end , : );

p = ( h * H' ) / ( h * h' );

e = [ 1 p ].' ;

for ii=1:length(elevation_range)
for jj=1:length(azimuth_range)

Ppdda(ii,jj) = abs( A(ii,jj)' * e ) )^2 ;

end
end


end
```

Table 2.1: Code for PDDA algorithm

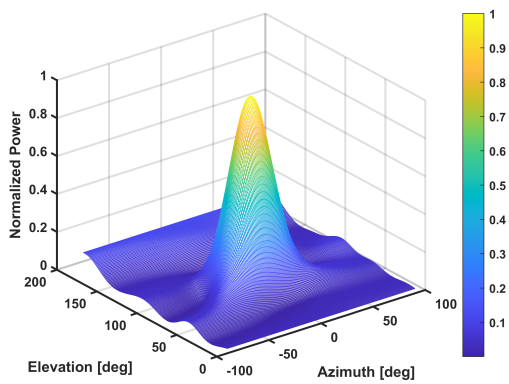

Figure 2.6: PDDA Pseudo-Spectrum.

2.5.2 Multiple Signal Classification (MUSIC)

In October 1979, the paper containing the MUSIC algorithm was published [29]. The idea behind this algorithm is the decomposition of the received signal's covariance matrix [35] and the separation of the observation space into noise and signal subspace. The basis of these subspaces are retrieved from the eigenvector matrix. Based on these two orthogonal subspaces, the spatial power spectrum can

be computed. After scanning the spatial power spectrum, the highest spectrum peaks will indicate the AOA.

Lets assume that a signal following the (2.8) model is received at an antenna array containing M elements. The MxM covariance function of the received signal is denoted as R_{rr} and it can be decomposed using the eigenvalue decomposition [7] expressed as,

$$\boldsymbol{R_{rr}} = \boldsymbol{Q_{ss}}\boldsymbol{\Lambda_{ss}}\boldsymbol{Q_{ss}}^{H} + \boldsymbol{Q_{ns}}\boldsymbol{\Lambda_{ns}}\boldsymbol{Q_{ns}}^{H}, \tag{2.16}$$

where Q_{ss} is the signal subspace, Q_{ns} is the noise subspace, unitary matrices, and Λ_{ss} and Λ_{ns} are the diagonal matrices containing the eigenvalues of the signal and noise respectively. Then, the spatial power spectrum is defined as,

$$P_{MUSIC}(\phi,\theta) = \frac{1}{\boldsymbol{A}(\phi,\theta)^{H}\boldsymbol{Q_{ns}}\boldsymbol{Q_{ns}}^{H}\boldsymbol{A}(\phi,\theta)}, \tag{2.17}$$

The spectral peak search will provide the signals' AOA estimation. The MUSIC algorithm is a high resolution algorithm but its accuracy can be affected by parameters such as the sensor array, the inter element distance and the estimation of the covariance matrix.

The following table (Table 2.1) and figure (Figure 2.7) show an example of MUSIC algorithm code and pseudo-spectrum.

MUSIC Algorithm

```
function [Pmusic] = MUSIC (M, elevation_range, azimuth_range, A, Received_signal)

Rrr = cov(Received_signal);

[Eigenvectors, Eigenvalues] = eig(Rrr);

En = Eigenvectors( : , M-1 : -1 : 1 );

for ii=1:length(elevation_range)
for jj=1:length(azimuth_range)

Pmusic(ii,jj) = abs ( 1 / A(ii,jj)' * En * En' * A(ii,jj) ) ;

end
end


end
```

Table 2.2: Code for MUSIC algorithm

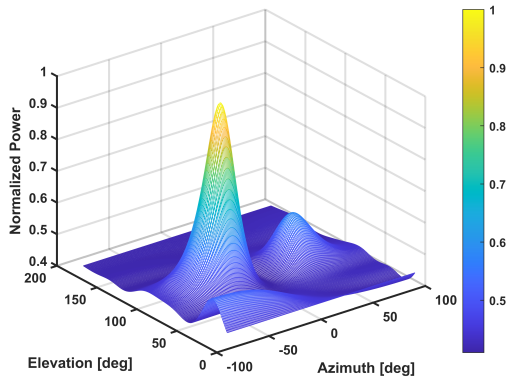

Figure 2.7: MUSIC Pseudo-Spectrum.

2.5.3 Subtracting Signal Subspace (SSS)

SSS is a method that exploits the orthogonality of the signal subspace and the Array Manifold Spectrum (AMV). From the perspective of computations, this method is efficient and can detect the DOA of the signals with any kind of antenna [6].
The process is similar to MUSIC algorithm. First, the correlation matrix of the received signal is calculated and then the eigenvalue decomposition is carried out as shown in (2.15) in order to extract the signal subspace $\boldsymbol{Q_{ss}}$. Finally, the SSS algorithm's pseudo-spectrum is given by,

$$P_{SSS}(\phi,\theta) = \left\| \boldsymbol{A}(\phi,\theta)^H \boldsymbol{Q_{ss}} \right\|^2, \tag{2.18}$$

The following table (Table 2.2) and figure (Figure 2.8) show an example of SSS algorithm code and pseudo-spectrum.

SSS Algorithm

```
function [Psss] = SSS (M, elevation_range, azimuth_range, A, Received_signal)


Rrr = cov(Received_signal);

[Eigenvectors, Eigenvalues] = eig(Rrr);

Es = Eigenvectors( : , M );

for ii=1:length(elevation_range)
for jj=1:length(azimuth_range)

Pss(ii,jj) = abs( norm ( A(ii,jj)' * Es ) )^2 ;

end
end


end
```

Table 2.3: Code for SSS algorithm

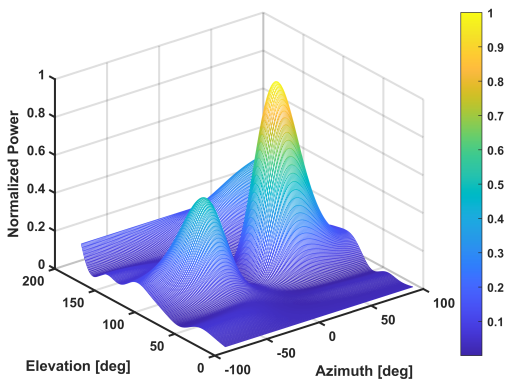

Figure 2.8: SSS Pseudo-Spectrum.

2.5.4 Estimation of Signal Parameters via Rotational Invariance Technique (ESPRIT)

The ESPRIT technique was introduced in 1989 [41] for the first time. The need to decrease the computational complexity demanded by positioning based applications caused the released of this technique brought by Richard Roy and Thomas Kailath. The main advantage of this technique compared with previous estimation methods like MUSIC relies on computation. As it will be shown in the derivation of this technique, ESPRIT eliminates the process of spatial search and the esti-

mation is purely based on the eigenvalues decomposition. Lets consider a 1xM+1 linear array and two M dimensional array data vectors defined as,

$$\boldsymbol{r_L}(t) = [r_1(t) \dots r_M(t)]^T, \tag{2.19}$$

$$\boldsymbol{r_U}(t) = [r_2(t) \dots r_{M+1}(t)]^T, \tag{2.20}$$

The received data model of (2.23) and (2.24) equations follow the (2.5) model. Then, the eigenvalue decomposition of the received signal's covariance matrix as shown in (2.15) is carried out in order to extract the signal subspaces according to both vectors, $r_L(t)$ and $r_U(t)$,

$$\boldsymbol{E_s} = \begin{bmatrix} \boldsymbol{E_{s,L}} \\ \boldsymbol{E_{s,U}} \end{bmatrix}, \tag{2.21}$$

According to both signal subspaces a new matrix $\boldsymbol{C}$ is defined of the following form,

$$\boldsymbol{C} = \begin{bmatrix} \boldsymbol{E_{s,L}}^H \\ \boldsymbol{E_{s,U}}^H \end{bmatrix} [\boldsymbol{E_{s,L}}, \boldsymbol{E_{s,U}}], \tag{2.22}$$

Again, an eigenvalue decomposition is performed over $\boldsymbol{C}$ matrix, whose partition is given by,

$$\boldsymbol{E_c} = \begin{bmatrix} \boldsymbol{E_{11}} & \boldsymbol{E_{12}} \\ \boldsymbol{E_{21}} & \boldsymbol{E_{22}} \end{bmatrix}, \tag{2.23}$$

where the indexes within E_c refer to the eigenvectors that correspond to the sorted eigenvalues, $\lambda_{11} \geq ... \geq \lambda_{22}$. Finally, the eigenvalue decomposition of the rotational operator (2.28) is done, and the estimated angle (2.29) is obtained.

$$\boldsymbol{\Psi} = -\boldsymbol{E_{12}}\boldsymbol{E_{22}}^{-1}, \tag{2.24}$$

$$\beta = \sin[\frac{c_0}{\omega_c d} \arg(\lambda_\Psi)] \tag{2.25}$$

where c_0 is the light speed, ω_c is the angular frequency, d is the separation between elements of the array and λ_Ψ is the dominant eigenvalue of $\boldsymbol{\Psi}$. An important conclusion that can be extracted looking at (2.29) is that ESPRIT algorithm is applied on ULAs and estimation in both azimuth and elevation planes is done by applying the algorithm independently in different ULAs within a URA.

ESPRIT Algorithm

```
function [AoA_ESPRIT] = ESPRIT (M, d, fc, Received_signal)


R_L = Received_signal( : , 1:(M-1) ).' ;
R_U = Received_signal( : , 2:M ).' ;

R = [ R_L ; R_U ];
Rrr = cov( R.' );

[Eigenvectors, Eigenvalues] = eig(Rrr);
Es = Eigenvector( : , (M-1)*2 );

Es_L = Es( 1 : M-1 , 1);
Es_U = Es( m : (M-1)*2 , 1);

C = [ Es_L' ; Es_U' ] * [ Es_L , Es_U ]

[Eigenvectors_C, Eigenvalues_C] = eig(C);
Eigenvector_C( : , 1 ) = Eigenvector_C_s( : , 2 )
Eigenvector_C_s( : , 2 ) = Eigenvector_C( : , 1 )

E12 = Eigenvector_C_s( 1 , 2 );
E22 = Eigenvector_C_s( 2 , 2 );

Psi = -E12 * (E22 ^-1);

[Eigenvector_psi, Eigenvalues_psi] = eig(Psi);

AoA_ESPRIT = (asin( (3e8 / (2*pi*fc*d)) * angle(Eigenvalue_psi) )) * (180/pi) ;
```

Table 2.4: Code for ESPRIT algorithm

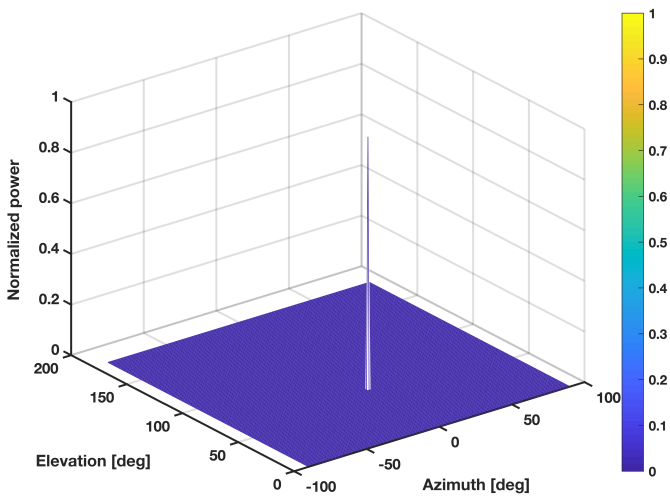

Figure 2.9: ESPRIT Pseudo-Spectrum.

2.6 Bluetooth Low Energy (BLE) v5.1

A device using Bluetooth v5.1 technology is able to locate the direction of the received signal more accurately than its predecessor versions. Previous indoor positioning systems based on RSSI applying trilateration [37] are now improved with BLE v5.1 who provides additional information like angular directions.

The direction finding feature offers two methods. The first one is AOD and the second one is AOA as mentioned above. Both methods use an antenna array that is connected to an RF switch. The difference in these methods is the positioning of the antenna array. In the former the element array is on the transmitter side and on the latter it is on the receiver side as can be seen in Figure 2.10. This approach is also known as virtual arrays [21]. The cost of this configuration is much lower compared to a real array [21] due to the necessity of not having a receiver module per antenna element. In addition, space is also saved, enabling the implementation of this configuration in small embedded devices.

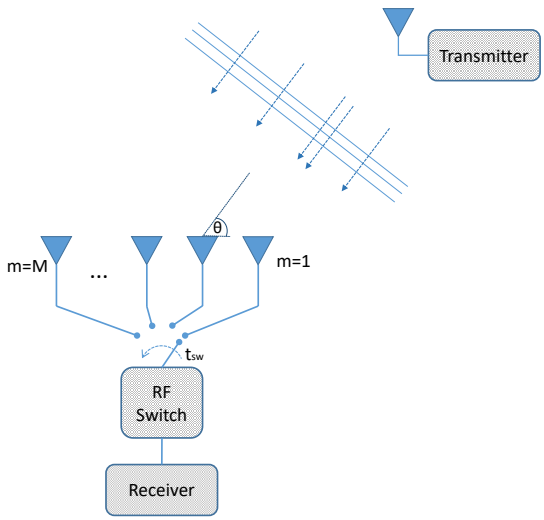

Figure 2.10: AOA Method

Regarding the protocol bit stream information, in BLE v5.1 a new link layer Protocol Data unit (PDU) has been defined for direction finding between two devices. The PDU has additional data known as Constant Tone Extension (Figure 2.11) which consist of binary 1's symbols whose length is predefined according to system requirements. Thus, the addition of the CTE to the PDU makes it feasible to sample a considerable amount of data required for later signal processing.

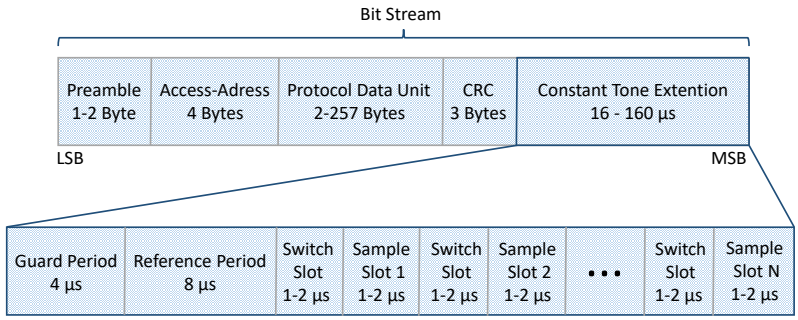

Figure 2.11: BLE signal with CTE

The duration time of CTE as shown in Figure 2.11 varies from 16-160 μs and that period is broke down into guard period, reference period and switching/sampling slots. As stated in Bluetooth Core Specification v5.1 the guard period is 4 μs, the reference period is 8 μs, and the sequence of switching slot and sampling slot can be 1 μs or 2 μs. The switching and sampling process is introduced in the *Data Acquisition* section.

A summary of the most important BLE v5.1 parameters [42] for this thesis is shown in Table 2.5 and the BLE frequency band, is presented in Figure 2.12 .

Bluetooth v5.1 Parameters	
Frequency Band	2.40 GHz - 2.48 GHz (ISM)
Total Bandwidth	80 MHz
Number of Channels	40
Channel Bandwidth	2 MHz
Sampling Rates	1 MS/s or 2 MS/s
Modulation Schemes	Binary FM (mandatory)
	$\pi/4$-DQPSK (optional)
	8-DPSK (optional)
Data Rates	1 Mbps (Binary FM)
	2 Mbps ($\pi/4$-DQPSK)
	3 Mbps (8-DPSK)

Table 2.5: BLE v5.1 parameters

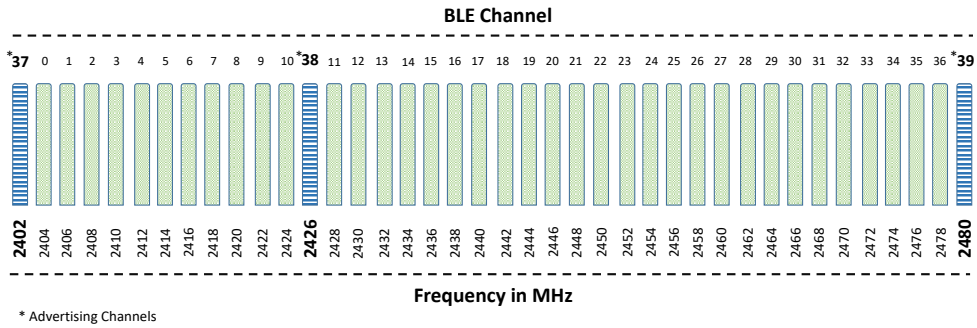

Figure 2.12: BLE frequency band

Chapter 3

Bluetooth v5.1 Direction Finding

In order to evaluate different AOA estimation algorithms, different measurements have been done with different setups. There are two different categories of measurements; direction finding measurements and virtual positioning measurements. All measurements are carried out inside an office building to comply with indoor conditions. In this chapter, prior to present the results of each scenario, an overview of the hardware and environments is introduced.

3.1 Hardware

The hardware used in the measurements consists of two modules, one for the receiver, and another one for the transmitter, both with BLE capabilities. Regarding the antennas, three different antenna arrays have been used at the receiver side and one antenna at the transmitter side mounted on tripods. Figure 3.1 shows the system with which the measurements were carried out.

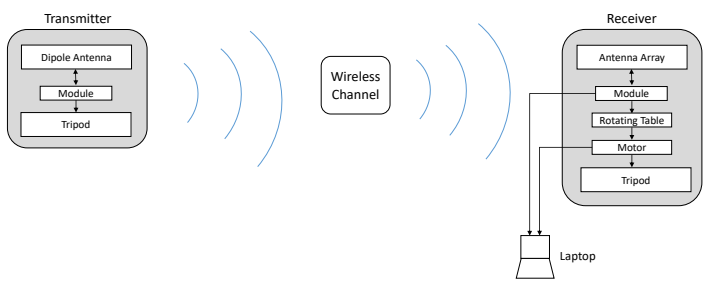

Figure 3.1: Hardware used in measurements

According to the antennas, three different antenna arrays have been used in the receiver. Two of them are URAs and one is a 12 elements square shaped antenna

array. The transmitter antenna is a common dipole with a constant transmitted power of 4 dBm for all measurements (Figure 3.3).
The 12 elements square shaped antenna is depicted in Figure 3.2c. Each element consists of a patch antenna and the vertical and horizontal distance between elements is 0.05 m. This antenna is still in the process to be launched to the market, so there is no official information about the radiation pattern for the moment. In the URA antennas, the same patch element is used in both arrays, 4x4 (Figure 3.2b) and 2x8 (Figure 3.2a). The difference relies on the distance between elements and the RF switching. In the 4x4 array the vertical and horizontal separation is 0.045 m and 0.04 m respectively, while in the 2x8 array the distances are 0.045 m and 0.03 m respectively. The per element radiation pattern is shown in Figure 3.4
.

(a) 2x8 URA antenna

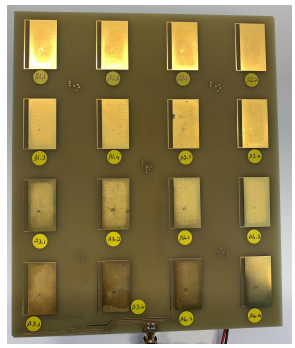

(b) 4x4 URA antenna

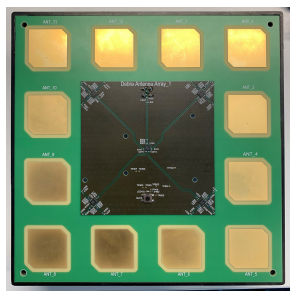

(c) 12 elements square shaped antenna

Figure 3.2: Antenna arrays

Figure 3.3: Transmitting dipole antenna

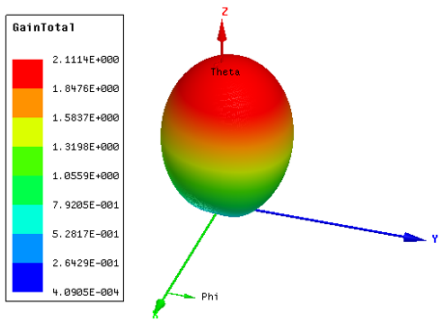

Figure 3.4: 4x4 and 2x8 per element radiation pattern

(a) Tx Module

(b) Rx module

Figure 3.5: *Ublox* Modules

According to the modules, the board used in the measurements is a *NINA-B4* [39] module mounted on a *EVK-NINA-B3* [40], both manufactured by *u-blox*.

The tripod on the receiver side has a rotating table with a 360° mobility. The reason for this is that for every measurements the receiving antenna has been rotated over a range of space as it is shown in Figure 3.6 from -80° to 80°. This is done in order to acquire the largest set of data possible for the post-processing analysis. The motor rotates the table in a pre established angular step size of 5°. Both the motor and the module are connected to a laptop via USB connection.

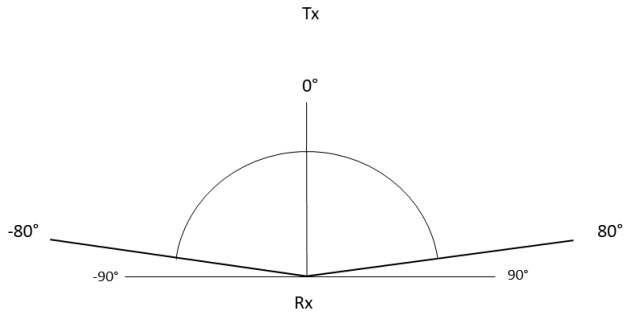

Figure 3.6: URAs rotation angle range

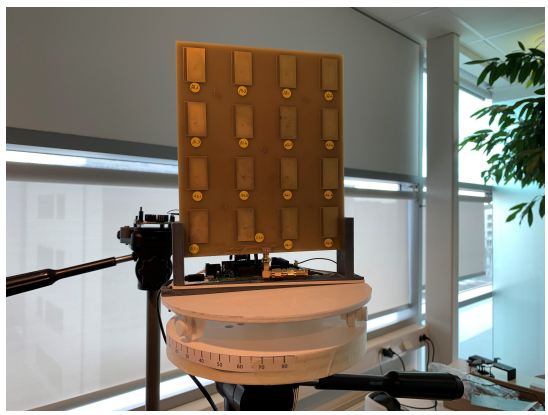

Figure 3.7: 4x4 URA antenna mounted on the rotating table

3.2 Data Acquisition

The measurements are initialized first by a python script which is in charge of acquiring the data from the antenna. The script is responsible of selecting the angular range of the measurements, the angular step size, and the number and length of CTE packets collected on each measurement. When a measurement is finished, the data is saved into a .txt file. This file contains CTE packets which besides the IQ samples, contains information about the frequency channel, the switching slot period, the sampling slot period, the sampling rate, the ground truth angle and the RSSI among others.
The received signal matrix $\mathbf{r}(t)$ is built by arranging the IQ samples such that an MxK matrix is obtained, where K refers to snapshots and is determined by the CTE packet length. Figure 3.8 depicts how the sampling sequence is configured for each antenna.

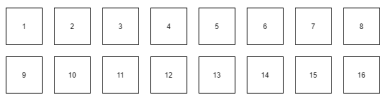

(a) 2x8 URA sequence

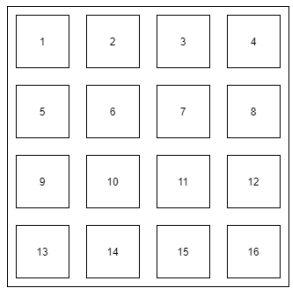

(b) 4x4 URA sequence

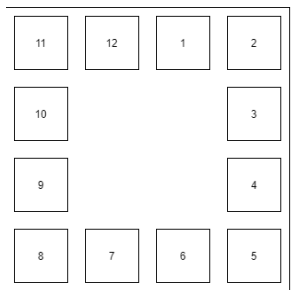

(c) 12 elements square shaped sequence

Figure 3.8: Switching/Sampling sequences

The acquired data consists of a predefined number of packets forming a data vector with samples corresponding to the reference, switching and sampling slots. The samples that belong to the switching slots needs to be discarded due to amplitude instabilities (Figure 3.9) while performing the switching from one element to the other. This instability leads to wrong angular estimations. Thus, as seen in the protocol (Figure 2.11) this periods can be 1 or 2 μs. We decided to set both periods at 2 μs. This means that the first half of the samples from each element will be discarded.

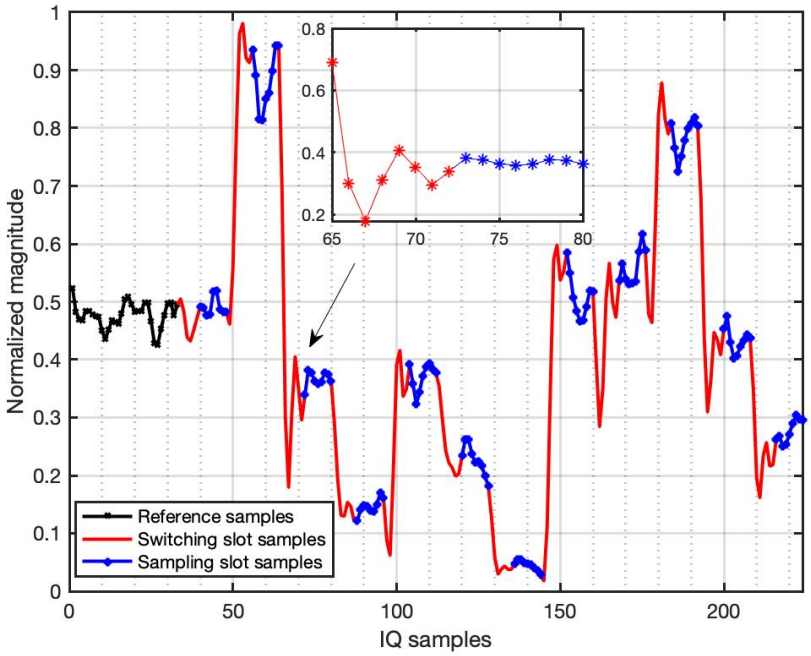

Figure 3.9: IQ samples from a CTE packet

Figure 3.9 shows the amplitude of the received IQ samples. The red colored transitions correspond to the switching slots samples while the blue colored samples belong to the sampling slots samples. It is clear here the difference between switching and sampling samples. This is a full sequence taken from the 12 elements square shaped antenna (Figure 3.2c).

3.3 Ground Truth Calculation

It is important to say that the ground truth is known for every measurement, since the rotating table has angle references in it and both the transmitter and receiver are aligned with each other. The set of spherical coordinates are also moved with the rotating table, i.e, the rotational angle is at ϕ=0° in spherical coordinates at every rotation (Figure 3.10).

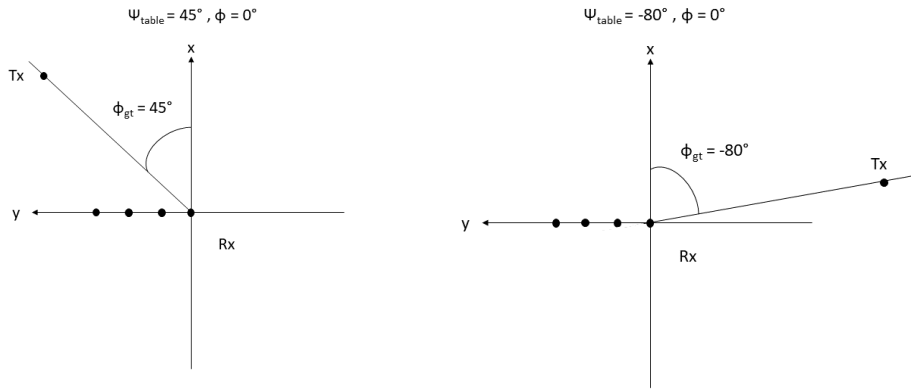

(a) Ground truth for 45° rotating angle

(b) Ground truth for -80° rotating angle

Figure 3.10: Ground truth for different rotating angles using the 4x4 URA

As it can be seen in Figure 3.10, the origin of the spherical coordinates is placed at the reference element of each antenna, i.e the first antenna in the sampling sequence of the array. ψ_{table} stands for the rotating angle, ϕ is the azimuth angle according to the spherical coordinates and ϕ_{gt} means the ground truth angle in azimuth according to the spherical coordinates. According to the elevation ground truth, since both the transmitter and the receiver are at the same height, the elevation ground truth will always be at θ=90°.

3.4 Bluetooth v5.1 Direction Finding Measurements

3.4.1 Scenario

The scenario where the measurements are taken is a dynamic indoor office environment. Figure 3.11 shows the scheme of these measurements. It is important to notice the surface differences between the right and left boundaries and the difference between the height and width boundaries (Figure 3.13).

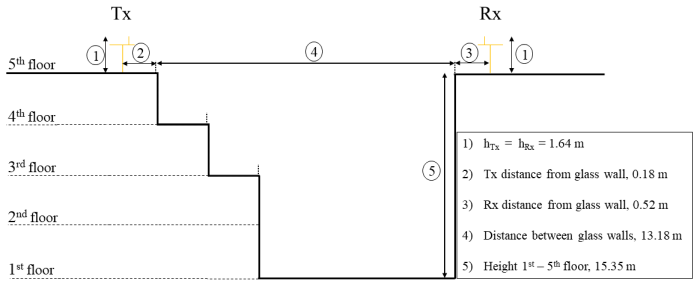

Figure 3.11: Long range scheme

(a) Glass wall **(b)** Irregular structure

Figure 3.12: Left and right views from the receiver

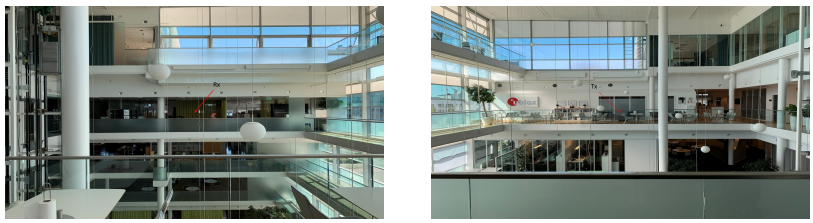

(a) View from the Tx side **(b)** View from the Rx side

Figure 3.13: Measurement scenario

The transmitter and the receiver are separated by a distance of 13.18 m and both are placed at 1.64 m height facing each other. Between the transmitter and the receiver there is a 15.35 m long courtyard. The fifth floor, where the measurements are taken, has a squared shaped corridor surrounding the area where there is an active human traffic. At the right side of the scenario from the receiver view there are two lifts who constitute an irregular surface and also an active source of movements.

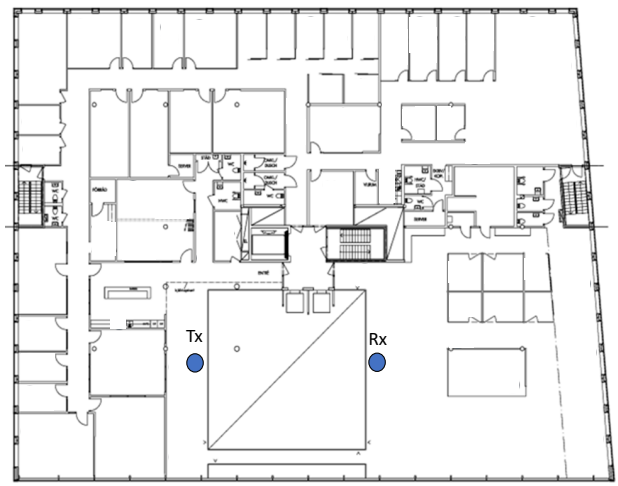

Figure 3.14: Floor plan

3.4.2 Objective

The objective of the direction finding measurements is to analyze the basics of AOA theory for a single receiving antenna array. Different evaluations are done regarding frequency diversity and AOA algorithm performance. According to frequency diversity, the measurements are carried out using three different frequencies in order to see whether the angular estimations are affected or not. According to AOA algorithms, PDDA, MUSIC, SSS and ESPRIT will be used to analyse the estimation performance and find a compensated algorithm in terms of computational effort and angular accuracy.

3.4.3 Frequency Effect on AOA Estimations

BLE v5.1 has 40 channels available to transmit. In order not to overlap with 802.11 bands, the BLE advertising channels (Figure 2.12) have been used. First we analyse whether the separation between these channels exceeds the coherence bandwidth and thus, gives us approximately independent fadings [21] which might impact the angular estimations.
To this end, Table 3.1 and Table 3.2 shows the long range measurement and post-processing parameters respectively.

Long Range Measurement Parameters	
Transmitted Power	4 dBm
Frequency	2.402 GHz (Channel 37)
	2.426 GHz (Channel 38)
	2.480 GHz (Channel 39)
CTE packet length	128 μs
Reference time	8 μs
Switching slots time	2 μs
Sampling slots time	2 μs
Sampling Rate	250 ns
Number of CTE packets per frequency channel	10
Number of receiver's orientation positions	33
Angular step size	5°

Table 3.1: Measurement parameters

Post-Processing Parameters	
Algorithm	PDDA
Arrays' orientation	zy plane
Spectrum's step size	1°
Azimuth range	$-90° \leq \theta \leq 90°$
Elevation range	$0° \leq \phi \leq 180°$

Table 3.2: Post-processing parameters

Once the measurements are done and the process of data acquisition and signal processing is completed we can analyse the received power at each frequency channel in the spatial range to see if there are power variations, i.e, independent fadings between frequency channels. The following results correspond to the RSSI of three advertising channels and the three receiving antenna arrays.

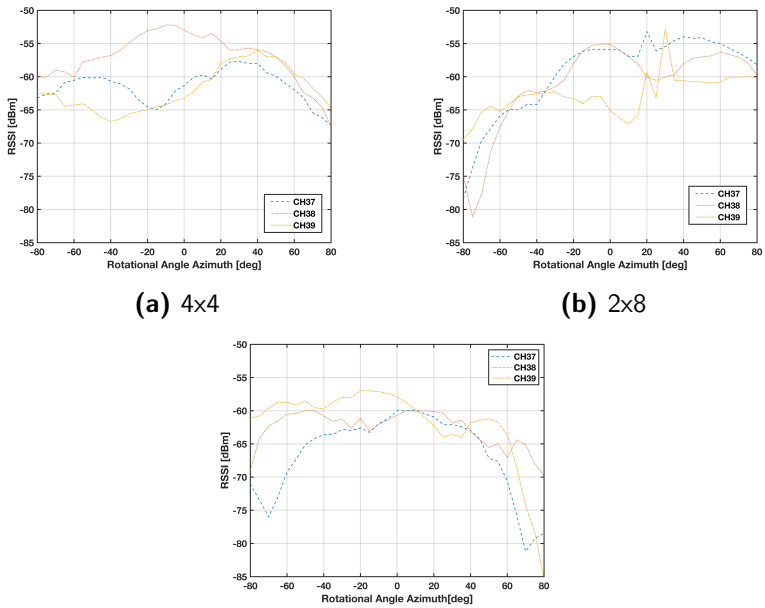

(a) 4x4 **(b)** 2x8

(c) 12 elements square shaped

Figure 3.15: RSSI values in the measured spatial range

First, it is clear how the RSSI values for each channel vary along the measured spatial range. This is obvious since the direction of maximum gain of the radiation pattern is moving in azimuth together with the rotating table and so the power will fluctuate along the spatial range. According to the RSSI level for different channels there is difference in power which means that each channel suffers from independent fading. Thus, we confirm that the coherence bandwidth does not exceed the bandwidth separation between the advertising channels and so there is frequency selectivity between 2.402 GHz, 2.426 GHz and 2.48 GHz channels.
Taking into account frequency selectivity, we can take advantage of it and use frequency diversity to ensure higher accuracy in AOA estimations for the described indoor scenario. To that end, the independent AOA estimation results for each frequency channel and antenna arrays are shown. These results are obtained using PDDA algorithm with the aim to show only the variations in AOA estimations according to different frequency channels.

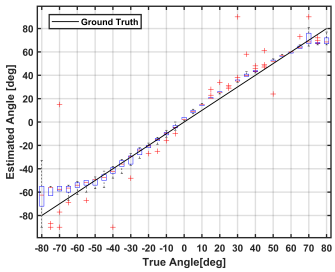

(a) Azimuth

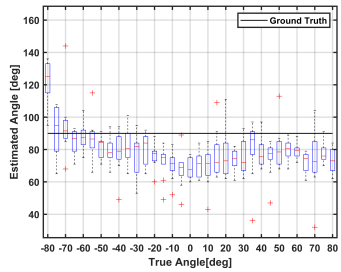

(b) Elevation

Figure 3.16: AOA estimation for 2x8 URA at Channel 37

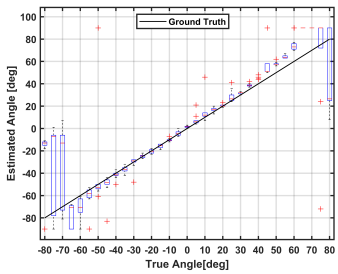

(a) Azimuth

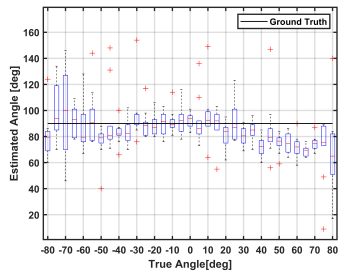

(b) Elevation

Figure 3.17: AOA estimation for 2x8 URA at Channel 38

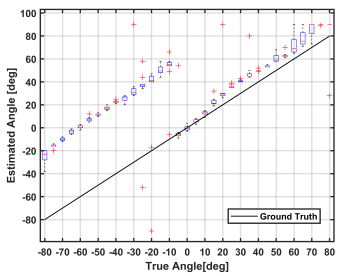

(a) Azimuth

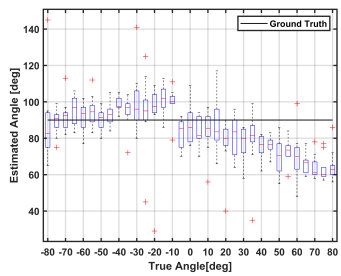

(b) Elevation

Figure 3.18: AOA estimation for 2x8 URA at Channel 39

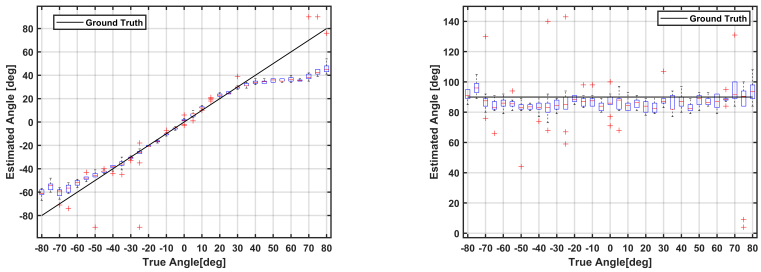

(a) Azimuth **(b)** Elevation

Figure 3.19: AOA estimation for 4x4 URA at Channel 37

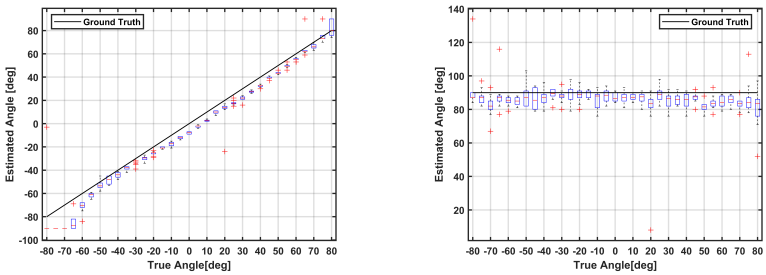

(a) Azimuth **(b)** Elevation

Figure 3.20: AOA estimation for 4x4 URA at Channel 38

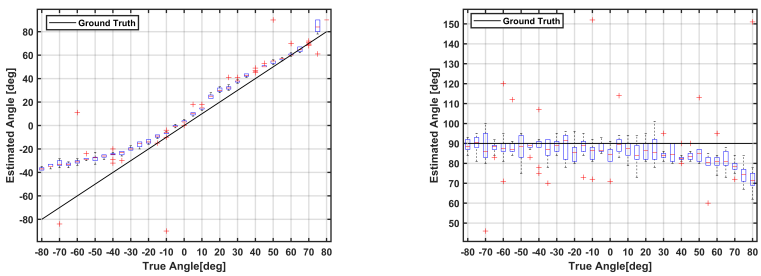

(a) Azimuth **(b)** Elevation

Figure 3.21: AOA estimation for 4x4 URA at Channel 39

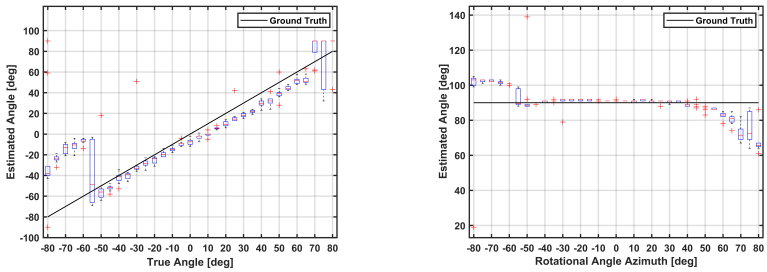

(a) Azimuth **(b)** Elevation

Figure 3.22: AOA estimation for 12 elements square shaped at Channel 37

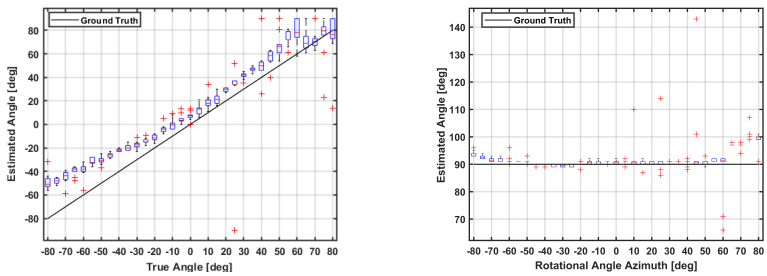

(a) Azimuth **(b)** Elevation

Figure 3.23: AOA estimation for 12 elements square shaped at Channel 38

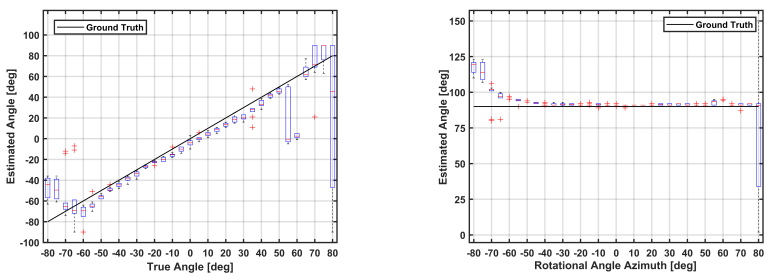

(a) Azimuth **(b)** Elevation

Figure 3.24: AOA estimation for 12 elements square shaped at Channel 39

Looking at the results, we confirm that the frequency in use impacts the angular estimations. However, the frequency of operation does not influence equally the estimations from different antenna arrays. The reason is that, first, the measurements were taken in a dynamic environment where people were moving around and thus the channel does not have the same response. Second, the antennas are not the same, their RF switching, reflection coefficient and radiation pattern differ from one to the other, leading to variations in angular estimations according to the frequency of operation. Thus, it is convenient to analyse the frequency effect within each antenna array.
According to 4x4 URA, we can see how in channel 37, the errors in AOA azimuth estimation are more pronounced at the right end of the space, while for channel 39 the estimations at the left side of the space are more affected. Channel 38 presents less pronounced errors at both sides of the space. Both extremes of the spaces are depicted in Figure 3.12. The left side of the space is conformed by a large glass wall with horizontal metallic bars while the right extreme of the space is composed by irregular surfaces with a corridor and two lifts on it. These difference in materials, surfaces and frequency leads to a different response in terms of the reflected power as it is explained by Fresnel's equations [21].
A very good example of material and surface reflectivity according to the frequency is given by analysing the 2x8 URA. As it can be seen in Figure 3.18a, we deduce that the estimated AOA when the antenna is facing the glass wall corresponds to a multipath component (MPC). The estimations taken from ten BLE packets do not present a high variance which means that there is certainty that the energy is been received from the same scatter area. Moreover, this scatter area remains static since the estimated AOA moves with the receiver's rotational angle. The reason why the antenna array obtains more power from the angle corresponding to the MPC than from the LOS direction relies on the radiation pattern. The patch antennas are characterized by having directive radiation patterns which affects the gain of the signals that are not being received around the direction of maximum gain. In this case, the reflected power at channel 39 and the antenna orientation results in having more power at the received MPC direction than in LOS direction.

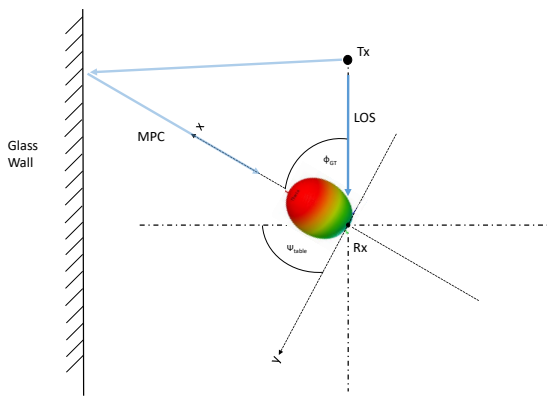

Figure 3.25: 2x8 URA two-path model at ψ_{table} = -65°

The distance between the transmitter and the receiver and the angle of incidence and reflection of the MPC in Figure 3.25 are not scaled. It is only an approximate illustration of what is happening at that specific rotational angle. To support and clarify this idea, the angular spectrums at ψ_{table}=-65°for different channel frequencies are shown in Figure 3.26.

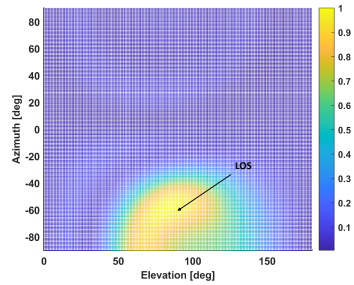

(a) Channel 37

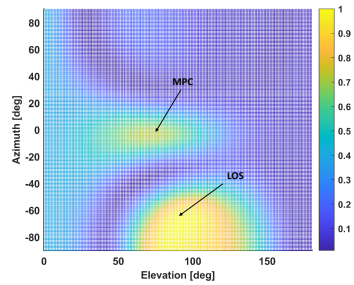

(b) Channel 38

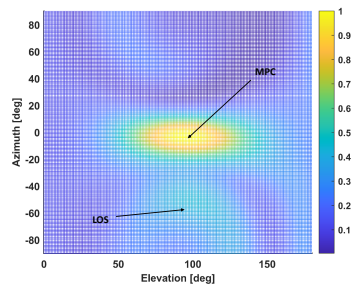

(c) Channel 39

Figure 3.26: Pseudo-spectrums of 2x8 URA at ψ_{table}=-65°

Looking at the angular pseudo-spectrums we can see how increasing the frequency of operation, the MPC that comes from the scatter gains more power. At channel 37 we only obtain energy from the LOS component, at channel 38 the major contribution comes from the LOS component but there is also energy corresponding

to the MPC. At channel 39 the energy of the LOS is almost vanished and the MPC collects the majority of the energy at the receiver. This has a huge impact in AOA estimation, since we are relying on peak search in the angular pseudo-spectrum. The angular estimation at channel 37 and channel 38 will stay close to the ground truth but the estimation at channel 39 will suffer a big deviation from the true angle since the major lobe corresponds to the MPC.

Thus, we conclude that the frequency channel used to transmit the BLE packet will impact the angular estimations. Prior to a BLE transmission there is no knowledge about channel information which leads to uncertainty in the angular estimations. However, if more than one frequency channels are used, the probability of having fading dips and incorrect angular estimations for all frequencies is drastically reduced. So, in the next section we propose an algorithm that exploits frequency diversity ensuring a robust angular estimation.

3.4.4 Proposed Algorithm for a Robust Angular Estimation using Frequency Diversity

The proposed algorithm will be explained using PDDA high resolution AOA estimation algorithm for simplicity purposes. The comparison between algorithms will be covered in next sections and they will be supported by this frequency diversity proposed algorithm.

The objective is to minimize as much as possible the incorrect estimations corresponding to a frequency channel. An incorrect estimation means that the algorithm has detected energy from a direction other than the true angle. It is important to notice that the measurements are in LOS scenario and so the correct estimation will correspond to a power peak detection of the LOS component in the angular spectrum. As seen in the 2x8 URA example of detecting the MPC as the DOA, we will not trust the pseudo-spectrum's amplitude for AOA estimations because of the radiation pattern's nature of patch antennas. Moreover, for that example we can also see how the RSSI level (Figure 3.15b) at the left side of the space for the MPC at channel 39 is higher than the LOS component at channel 37 and channel 38. This is the reason why we will not introduce the pseudo-spectrum's power for different frequency channels as a confidence parameter for the algorithm. To remove that dependency we propose normalizing the amplitude of the pseudo-spectrums. As we are using ten BLE packets for each ground truth we obtain ten normalized pseudo-spectrums. Now it is not the interest in how the AOA accuracy varies with the number of BLE packets tranmsitted. That evaluation will be analysed in next chapters. Thus, no matter the number of BLE packet used, the next step consists of averaging the normalized pseudo-spectrums. This is done in order to lower the power of possible unwanted peaks coming from MPCs that may appear in time. Once we obtain the average of N number of BLE packets' pseudo-spectrums of a frequency channel, it is now the time to make a frequency average between the three advertising channels. This average will reduce again the influence of the MPC's received power. To ilustrate this concept Figure 3.27a shows the pseudo-spectrum for different channels and Figure 3.27b shows the averaged pseudo-spectrum.

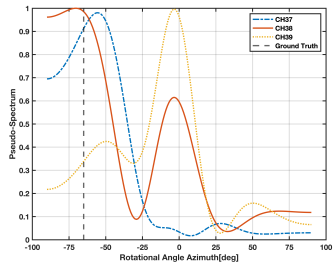

(a) Pseudo-spectrum of each channel

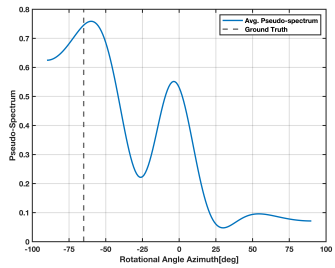

(b) Averaged pseudo-spectrum

Figure 3.27: Azimuth pseudo-spectrums of 2x8 URA at ψ_{table}=-65°and θ=92°

The pseudo-spectrums depicted in Figure 3.27 correspond to the power in the azimuth angles when the elevation is equal to θ=92°. We are using a 3D angular pseudo-spectrums but in order to clearly show the effect of the averaging a cut is made at θ=92°where there is an estimated peak in the elevation plane. We can see the importance of normalizing and averaging, giving equal weight to the three frequencies so that the power of the LOS component outperforms the MPC in the averaged pseudo-spectrum.

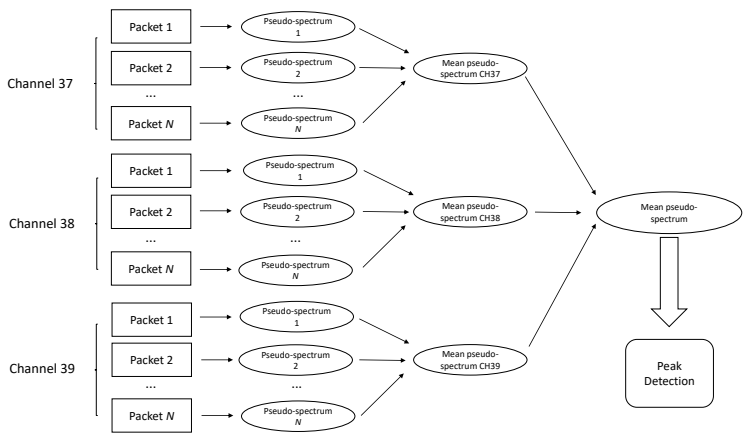

Figure 3.28: Proposed algorithm's diagram

The proposed algorithm's diagram is depicted in Figure 3.28. There is only one peak scanning in the algorithm and it is done in the final averaged pseudo-spectrum. This reduces computation complexity since the peak search is a computationally demanding operation.
The results of implementing this algorithm in the signal-processing is given by Figure 3.29, Figure 3.30 and Figure 3.31. At first sight, we see how the big vari-

ance and the incorrect estimations given from Figure 3.16 to Figure 3.24 are highly reduced using the proposed algorithm. Thus, a robustness in angular estimation accuracy is achieved with this algorithm. Going into specific details, the previously mentioned effect of channel 39 (Figure 3.18a) in the 2x8 URA within the first half of the space is completely reduced as it can be seen in Figure 3.29a. The improvement can also be demonstrated with the Mean Absolute Error (MAE) between individual channels (Table 3.3) and the final proposed algorithm's estimations (Table 3.4).
Looking at the MAE results, we can see how the algorithm obtains similar or better angular accuracy compared to the best performing channel. The MAE complies with the quality condition stated in this thesis with an angular accuracy less than 10°. The only parameter that does not comply with the condition is the MAE of 2x8 URA in elevation. The reason is that this array has only 2 elements on the elevation plane and it is not enough to achieve an accuracy less than 10°.

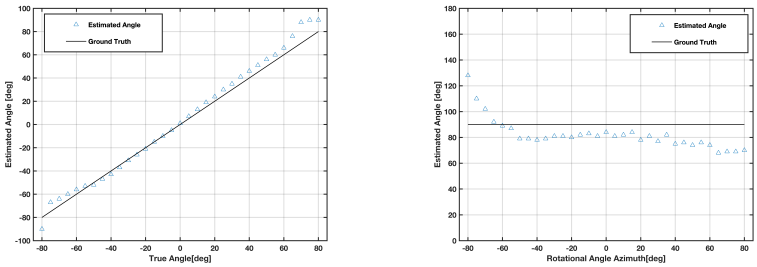

(a) Azimuth **(b)** Elevation

Figure 3.29: AOA estimation using the proposed algorithm for 2x8 URA

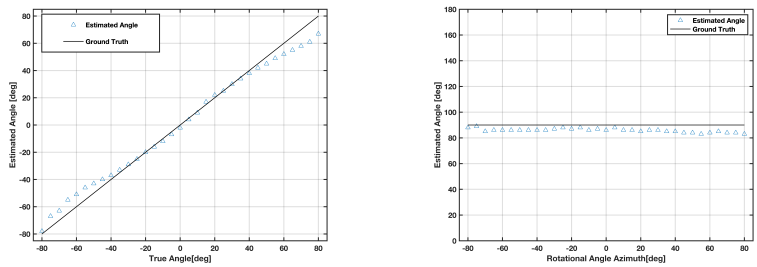

(a) Azimuth **(b)** Elevation

Figure 3.30: AOA estimation using the proposed algorithm for 4x4 URA

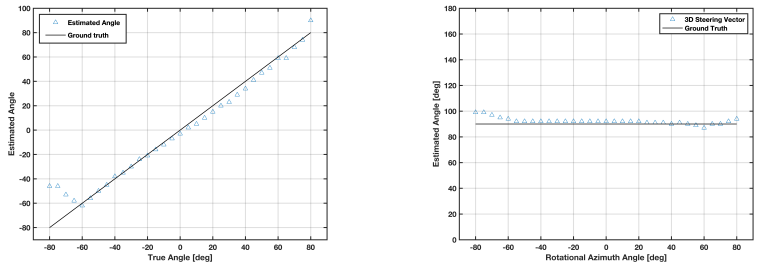

(a) Azimuth **(b)** Elevation

Figure 3.31: AOA estimation using the proposed algorithm for 12 elements square shaped

Mean Absolute Errors (°)			
		Azimuth	Elevation
2x8 URA	Channel 37	4.27	12.93
	Channel 38	8.72	9.57
	Channel 39	30.51	10.24
4X4 URA	Channel 37	9.42	4.21
	Channel 38	6.93	3.84
	Channel 39	12.51	4.75
12 elements square shaped	Channel 37	16.63	5.09
	Channel 38	14.12	1.57
	Channel 39	10.33	2.72

Table 3.3: MAE for individual channels

Mean Absolute Errors (°)		
	Azimuth	Elevation
2x8 URA	4.72	12.33
4X4 URA	4.54	4.21
12 elements square shaped	5.30	1.78

Table 3.4: MAE using the proposed algorithm

However, there is still a higher error at the extremes of the spatial range where the rectangular patch arrays loss efficiency due to directive radiation pattern. A possible solution to avoid this problem is to use spatial diversity. The use of more receivers increases the probability that a rectangular array will capture the energy around the direction of maximum gain and it also helps to increase the estimation robustness in OLOS and NLOS scenarios. This multiple receiver positioning system will be evaluated in next chapters.

3.4.5 DOA Estimation Algorithm Comparison

The comparison between DOA estimation algorithms will be carried out on top of the proposed algorithm that exploits frequency diversity. Since algorithms accuracy is affected by parameters such as antenna array, inter element distance and number of elements among others, it is unreasonable to make a discussion about the DOA algorithms performance across the antenna used. Thus, we will first compare them individually. To do so, the post-processing parameters used to evaluate the DOA estimation algorithms are shown in Table 3.5.

Post-Processing Parameters	
Algorithm	PDDA
	MUSIC
	SSS
	ESPRIT
Arrays' orientation	zy plane
Spectrum's step size	$1°$
Azimuth range	$-90° \leq \theta \leq 90°$
Elevation range	$0° \leq \phi \leq 180°$
Number of BLE packets	10
Number of snapshots	16

Table 3.5: Post-processing parameters

Once the implementation of the DOA estimation algorithms is done, first an overview of the results is introduced. Figure 3.32, Figure 3.33 and Figure 3.34 show the estimated angles over the true angles for PDDA, MUSIC, SSS and ESPRIT algorithms. At first view, it is noticeable the difference in angular estimation between ESPRIT and the rest of algorithms. These algorithms are implemented together with the proposed algorithm to improve the accuracy robustness. We explained how the algorithm works and how we are taking advantage of the pseudo-spectrums at different channels so that we enforce the LOS power over the MPCs. ESPRIT can not take advantage of this algorithm since it is giving the estimated angle and not the angular pseudo-spectrum. The consequence of this is the inability to differ peaks with different energies and thus penalize the averaged estimation from different channels. Furthermore, ESPRIT is performed over linear arrays and thus an average should be utilized on all the estimations corresponding to the rows and columns resulting in a less accurate angular estimation. This is happening because all the elements do not have the same performance due to manufacturing imperfections and can provide slightly different estimations. Thus, we assume here channel knowledge when implementing ESPRIT. The frequency channel that provides the best MAE result will be used in order to introduce it in this DOA algorithms discussion.

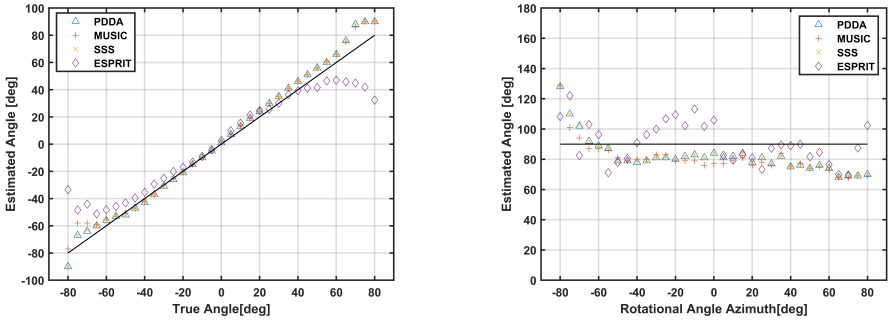

(a) Azimuth **(b)** Elevation

Figure 3.32: DOA algorithms in 2x8 URA

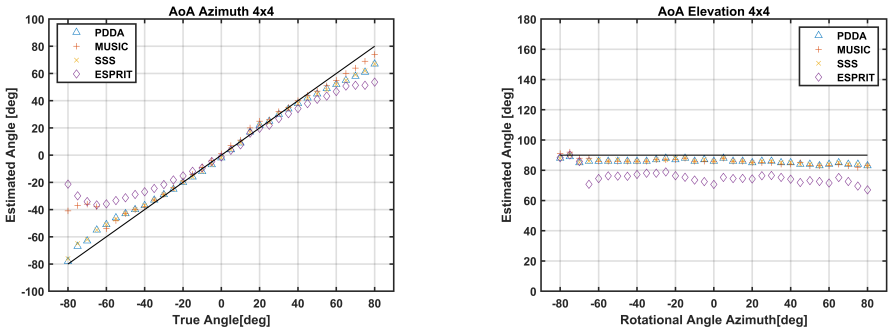

(a) Azimuth **(b)** Elevation

Figure 3.33: DOA algorithms in 4x4 URA

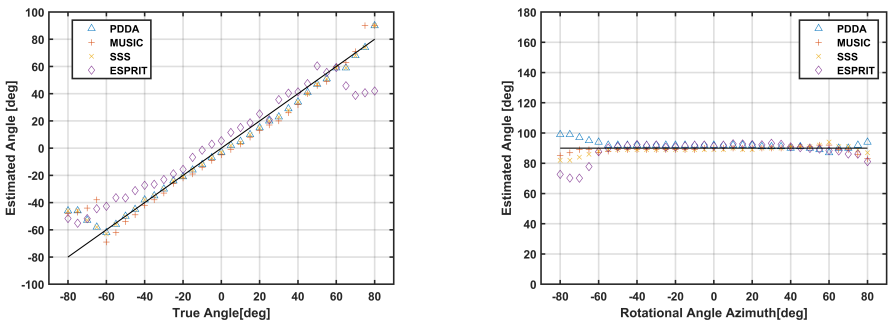

(a) Azimuth **(b)** Elevation

Figure 3.34: DOA algorithms in 12 elements square shaped

On the other hand, PDDA, MUSIC and SSS have very close estimations as expected in a LOS scenario. It is interesting to see how PDDA and SSS estimations are almost identical since the nature of the algorithm is different. Diverse evaluations will be made to see at which extent PDDA and SSS are close to each other. Table 3.6 reveals the MAE value corresponding to the used DOA algorithms for each antenna.

Mean Absolute Errors (°)			
		Azimuth	Elevation
2x8 URA	PDDA	4.72	12.33
	MUSIC	4.90	12.69
	SSS	4.69	12.33
	ESPRIT	10.81	11.24
4X4 URA	PDDA	4.15	4.21
	MUSIC	6.84	4.39
	SSS	4.66	4.12
	ESPRIT	12.51	4.31
12 elements square shaped	PDDA	5.30	1.78
	MUSIC	8.21	1.33
	SSS	5.33	1.75
	ESPRIT	11.89	3.62

Table 3.6: MAE for individual DOA algorithms

The MAE results are promising as we are complying with the condition of an error accuracy less than 10° for the system proposed. A way to compare an analyze the performance of DOA algorithms is to evaluate the pseudo-spectra provided by them. The next set of figures correspond to the pseudo-spectra for each DOA estimation algorithm and for each receiving antenna array at $\psi_{table} = 0°$. In order to visualize the estimations given by ESPRIT in a pseudo-spectrum format, we have given the estimated angle all the energy. So in the figures, the AOA can be seen as a unique dot with a normalized power equal to 1.

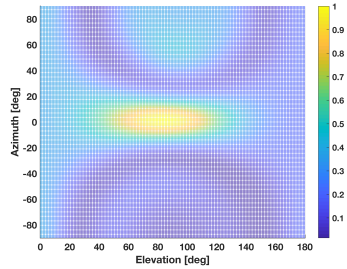

(a) PDDA

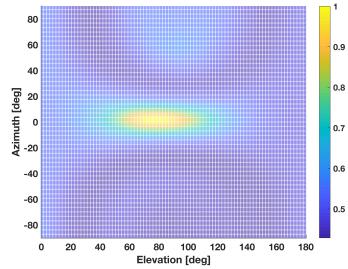

(b) MUSIC

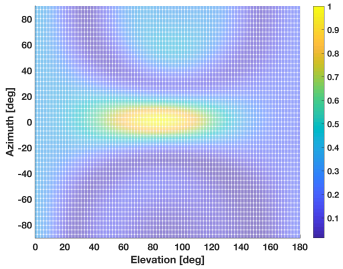

(c) SSS

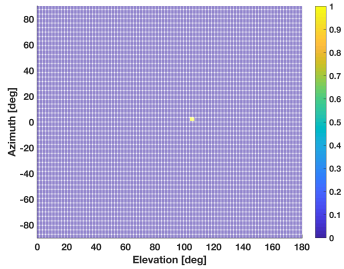

(d) ESPRIT

Figure 3.35: DOA algorithms in 2x8 URA

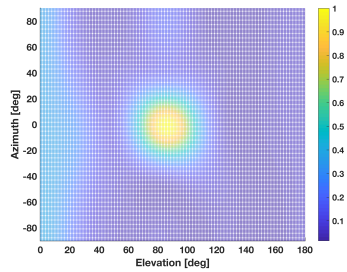

(a) PDDA

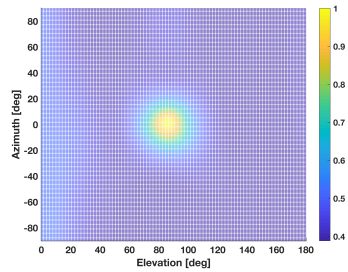

(b) MUSIC

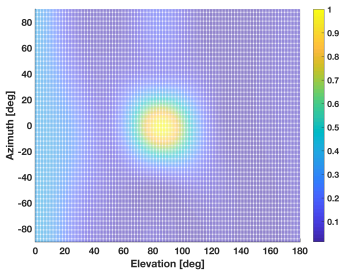

(c) SSS

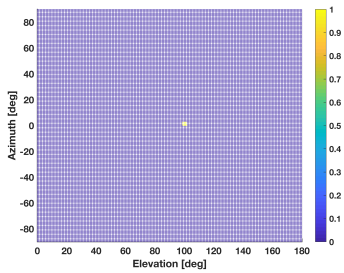

(d) ESPRIT

Figure 3.36: DOA algorithms in 4x4 URA

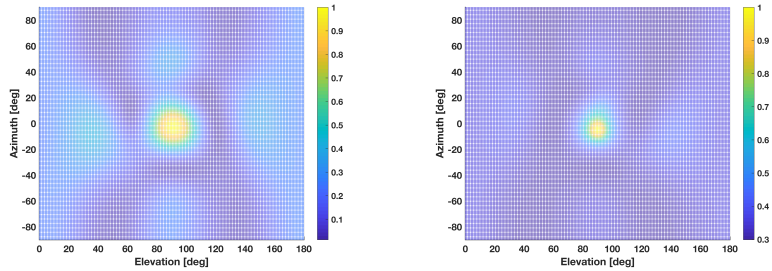

(a) PDDA **(b)** MUSIC

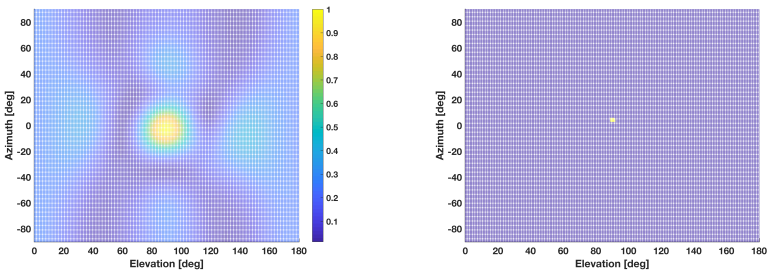

(c) SSS **(d)** ESPRIT

Figure 3.37: DOA algorithms in 12 elements square shaped

By looking at the pseudo-spectra, we see how the main lobe of the 2x8 URA differs from the main lobes of the rest of antenna arrays. It tends to an eliptical shape where the energy from the elevation plane is less resolved than the energy from the azimuth plane. This is due to the fact that 2x8 URA antenna has four times the elements in the azimuth plane than in the elevation plane. Thus, this results in a pseudo spectra with higher resolution in azimuth than in elevation. On the other hand, the main lobe of pseudo-spectra of 4x4 URA and 12 elements square shaped antenna have the same resolution in azimuth and elevation since the number of elements in both planes is the same.
In all three antennas, it can be observed that the pseudo-spectra of PDDA and SSS are indistinguishable in this LOS scenario. This is also supported with the MAE results for PDDA and SSS in all three arrays with very close results. Noticeable as well, in all antennas, a slightly higher resolution of the main lobe of MUSIC pseudo-spectra compared to PDDA and SSS. However, this higher resolution does not mean higher angular accuracy as it can be seen in Table 3.6. In fact, looking at the amplitude of MUSIC pseudo-spectra we see how the minimum received power is approximately 35% higher than in PDDA and SSS pseudo-spectra. This means that the noise floor is higher using MUSIC algorithm. The reason behind this might be the usage of the noise subspace by MUSIC algorithm resulting in a higher noise floor in the pseudo-spectrum. This can be verified implementing a simulation of the system and comparing it with the measured pseudo-spectra.

In order to proceed with the simulated version of the system the following parameters have been used together with the presented received signal model for arrays.

Simulation Parameters	
Algorithm	PDDA
	MUSIC
	SSS
Arrays' orientation	zy plane
Spectrum's step size	1°
Azimuth range	$-90° \leq \theta \leq 90°$
Elevation range	$0° \leq \phi \leq 180°$
Number of snapshots	1
Received signal model	$\mathbf{r} = \mathbf{a}\mathrm{s} + \mathbf{n}$
Number of sources	1
Transmitted signal	s = [1]
Noise	complex AWGN
AOA in azimuth	0°
AOA in elevation	90°

Table 3.7: Simulation parameters

In the simulation, the three advertising channels have been used together with the proposed algorithm that improves angular error robustness. Furthermore, an incoming signal direction at ϕ=0°and θ=90°is simulated so that we compare the simulation with the least disturbed position in the measured scenario with low or no MPC appearances. This orientation is also selected in order to minimize the effect of the radiation patterns and have the direction of maximum gain of the patch aligned with the transmitter. The simulation is done using different SNR levels in order to see how the algorithms are affected under noisy cases.

First of all, to compare how the SNR level impacts the algorithms pseudo-spectrum, Figure 3.38 is presented. At first sight we see how the lower level of SNR the higher noise floor appears in MUSIC pseudo-spectrum. This phenomenon do not manifests in PDDA and SSS pseudo-spectra. MUSIC algorithm makes use of the noise subspace which results in variations of the noise floor and resolution in the pseudo-spectrum. On the other hand, PDDA and SSS do not make use of the noise subspace which makes them more robust in terms of noise floor as it can bee seen in Figure 3.38a and Figure 3.38c. We can estimate the measured SNR level by analysing the MUSIC pseudo-spectrum. As it can be seen, the measured pseudo-spectrums' noise floor is between 1dB and 5dB of simulated SNR levels. Therefore we can induce that the received approximate SNR level is below 5dB.

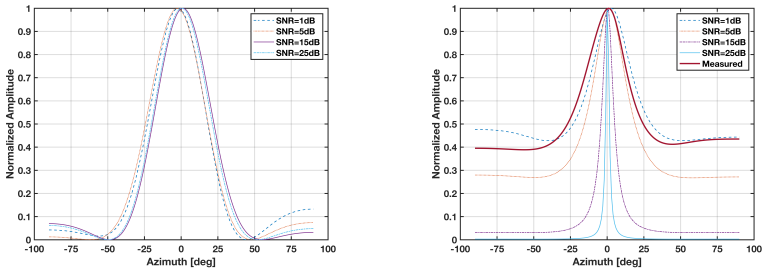

(a) PDDA

(b) MUSIC

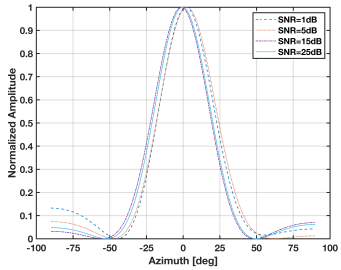

(c) SSS

Figure 3.38: Simulated DOA algorithms with different SNR levels for 4x4 URA

The next figure shows the three algorithms for a SNR level of 3dB. We confirm the measured similarities between PDDA and SSS pseudo-spectra. The simulated version of the system also supports the concept of equivalence between PDDA and SSS algorithms.

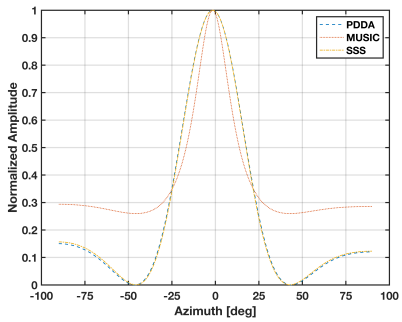

Figure 3.39: Simulated DOA algorithms for 4x4 URA and SNR=3dB

Figure 3.40, Figure 3.41 and Figure 3.42 depict the comparison between the simulated version of the system and the measured data. It is noticeable how close the simulated pseudo-spectra and the measured pseudo-spectra are, which means that the proposed direction finding system is successfully implemented. However, there are some differences specially in the secondary lobes. This is due to the impact of the statistical fluctuation of the noise at low SNR.

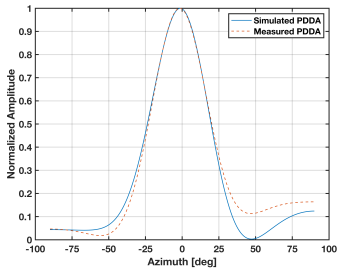

(a) PDDA

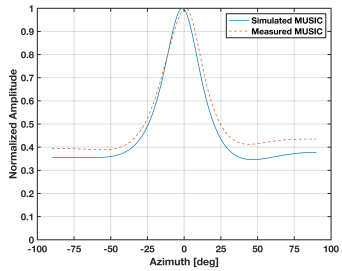

(b) MUSIC

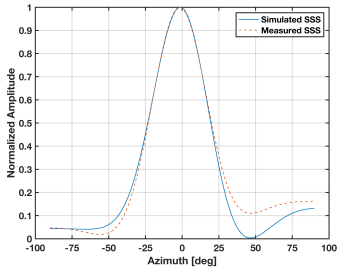

(c) SSS

Figure 3.40: Comparison between DOA simulated algorithms and measured data for 4x4 URA and SNR=3dB

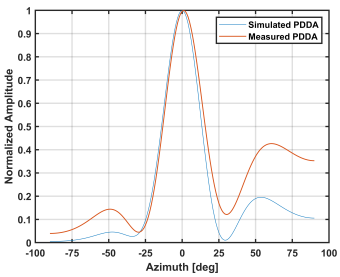

(a) PDDA

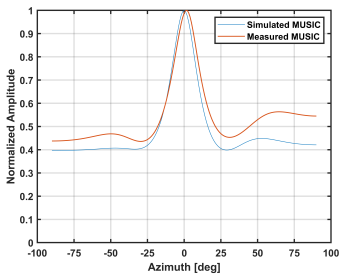

(b) MUSIC

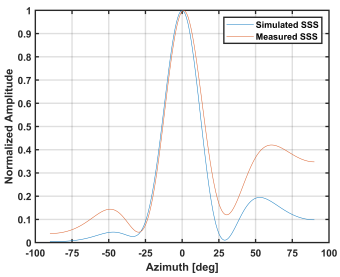

(c) SSS

Figure 3.41: Comparison between DOA simulated algorithms and measured data for 2x8 URA and SNR=1dB

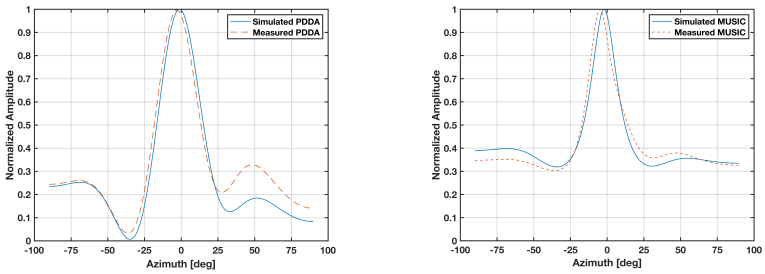

(a) PDDA **(b)** MUSIC

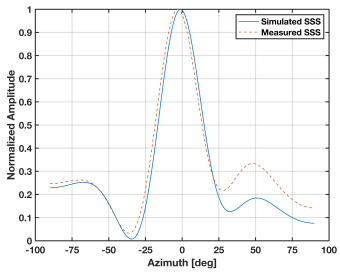

(c) SSS

Figure 3.42: Comparison between DOA simulated algorithms and measured data for 12 elements square shaped and SNR=1dB

We still need more analysis in order to reach the conclusion of which algorithm is more compensated in terms of computation complexity. To do so, we present five different evaluations to push the algorithms to extreme cases and obtain the best compensated algorithm. These evaluations are based on analysing the MAE results with different number of antenna elements, different number of received BLE packets, number of snapshots, pseudo-spectrum's angular step size and the elapsed time by each algorithm.

Antenna Elements

In this evaluation, the MAE will be examined in terms of the number of elements used on each antenna for each DOA algorithm. The same post-processing parameters of Table 3.5 are applied. The next set of figures show the evaluation of the MAE according to the number of elements used for each antenna.

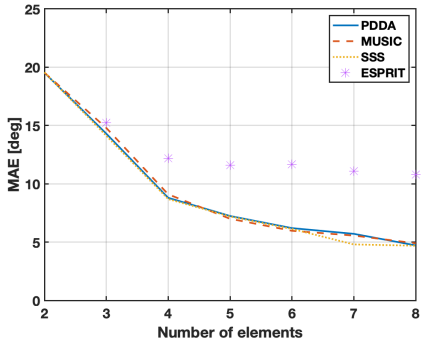

Figure 3.43: 2x8 URA element evaluation

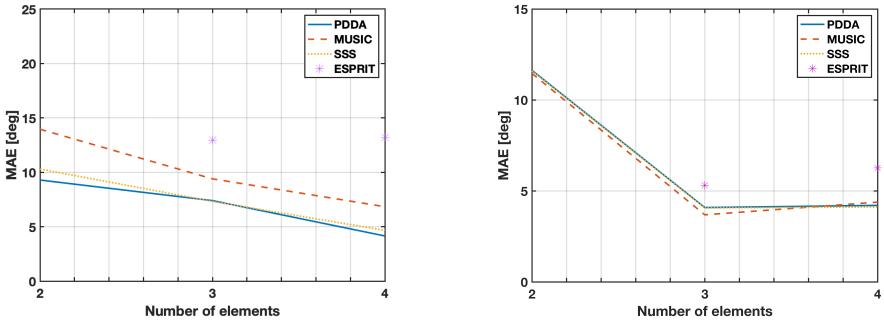

(a) Azimuth **(b)** Elevation

Figure 3.44: 4x4 URA element evaluation

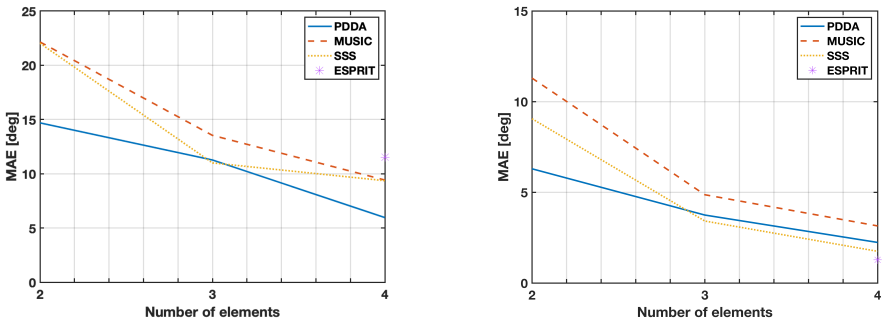

(a) Azimuth **(b)** Elevation

Figure 3.45: 12 elements square shaped element evaluation

MAE (°)							
	Azimuth						
Number of Elements	2	3	4	5	6	7	8
PDDA	19.53	14.30	8.8	7.24	6.2	5.71	4.72
MUSIC	19.54	14.79	9.1	7	5.97	5.56	4.90
SSS	19.56	14.12	8.69	7.2	6.13	4.8	4.69
ESPRIT	-	15.24	12.20	11.60	11.66	11.08	10.81

Table 3.8: 2x8 URA MAE with different number of elements

MAE (°)						
	Azimuth			Elevation		
Number of Elements	2	3	4	2	3	4
PDDA	9.29	7.4	4.15	11.63	4.09	4.21
MUSIC	13.96	9.4	6.84	11.46	3.69	4.39
SSS	10.3	7.33	4.66	11.6	4.07	4.12
ESPRIT	-	12.97	12.51	-	5.31	4.31

Table 3.9: 4x4 URA MAE with different number of elements

MAE (°)						
	Azimuth			Elevation		
Number of Elements	2	3	4	2	3	4
PDDA	14.69	11.27	5.96	6.3	3.75	2.24
MUSIC	22.15	13.54	9.42	11.3	4.87	3.15
SSS	22.03	11	9.36	9.06	3.42	1.75
ESPRIT	-	-	11.53	-	-	1.28

Table 3.10: 12 elements square shaped MAE with different number of elements

As expected, the MAE is reduced using more antenna elements. In some cases, ESPRIT can not be implemented in the system. The reason is that standard ESPRIT is composed by complex-valued computations and in some cases the estimation is given by a non valid complex number, as it is happening when small number of elements are used. A future line of this thesis is to get rid of complex estimations using centro-symetric arrays which give real valued signal subspace. This process is part of the Unitary-ESPRIT algorithm. Apart from that, observable is the fact that the performance of PDDA and SSS is almost exact with small differences across the range of the elements. Considering the MAE threshold of 10°, we can conclude that a less number of elements can be used in the antennas. For 4x4 URA, three elements in azimuth and elevation can be used together with PDDA,

SSS or MUSIC and still comply with the error condition. For 12 elements square shaped, the number of elements in elevation can be reduced to three elements. Finally, for 2x8 URA the MAE is under 10° using 4 elements. This is important as hardware and computational complexity is reduced.

Number of BLE Packets

In this evaluation, the Mean Absolute Error using the DOA algorithms will be analysed in terms of number of BLE packets used for the estimation. The initial post-processing parameters (Table 3.5) will be followed except for the number of BLE packets that will vary from one to ten packets. The full array is used for every antenna. We present the result only for 12 elements square shaped antenna since the same behavior is observed for the URAs. Figure 3.46 shows the evaluation of the MAE over the number of BLE packets used.

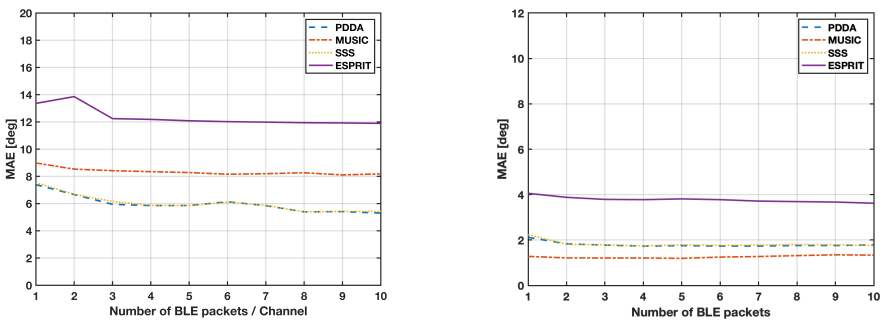

(a) Azimuth **(b)** Elevation

Figure 3.46: MAE vs BLE packets used for 12 elements square shaped

As it can be seen in Figure 3.46, the performance in terms of MAE is practically constant for PDDA, MUSIC, SSS and PDDA over the number of BLE packets used. Thus, we can conclude that we can use a less number of BLE packets for angular estimations in order to achieve less than 10°of MAE when using the DOA algorithms. The benefit of using a less amount of packets relies on a shorter computation time that takes for an angular estimation and making it feasible to implement it in fast-response real time scenarios. However, a margin should be left in the minimum number of packets in case of possible bits corruption in the BLE packet.

Number of Snapshots

In this evaluation, we analyse how the MAE is affected by using a different amount of snapshots. Having less number of snapshots means that the correlation matrix of the received signal will be built under less amount of samples which makes it less accurate. SSS, MUSIC and ESPRIT make use of the correlation matrix and might be affected by a less number of snapshot for angular estimation. Figure 3.47 show

the MAE over the number of snapshots used for each one of the DOA algorithms in 12 elements square shaped. The MAE remains approximately constant over the number of snapshots used. This tendency is also happening in 2x8 and 4x4 URAs. Thus, angular estimation can be performed with only one snapshot, which shortens the data acquisition process.

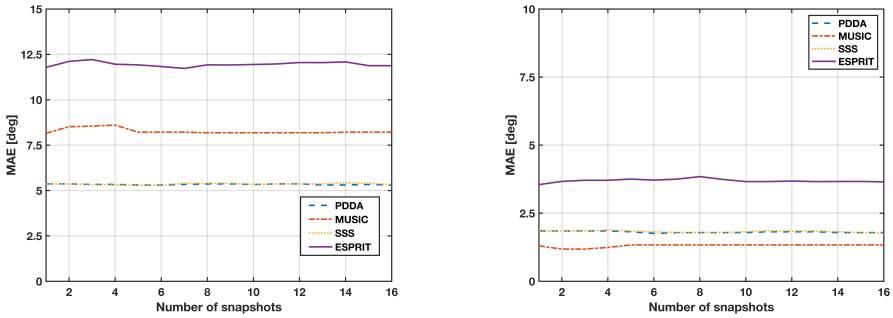

(a) Azimuth **(b)** Elevation

Figure 3.47: MAE vs snapshots for 12 elements square shaped

Pseudo-Spectrum Angular Step Size

As for the previous evaluation, we will rely on the MAE results from the DOA algorithm to investigate their performance when the spectrum step size is changing. The same post-processing parameters are applied here as above, with the exception of the the spectrum's step size. The range of the spectrum step size is from 0.5° to 20° with a step of 0.5°. We used an upper bound of 20° in the spectrum step size to limit the error in the elevation plane to 10°. The results are demonstrated in the following figures.

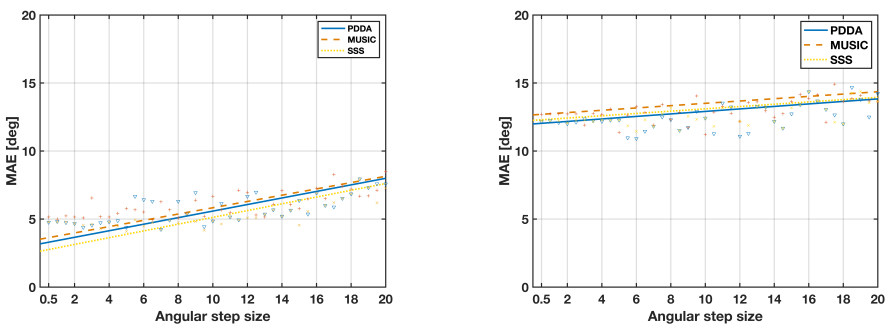

(a) Azimuth **(b)** Elevation

Figure 3.48: 2x8 URA for different angle step size

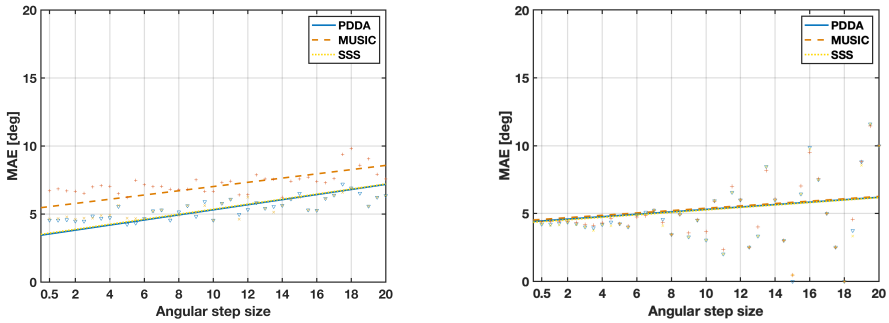

(a) Azimuth **(b)** Elevation

Figure 3.49: 4x4 URA for different angle step size

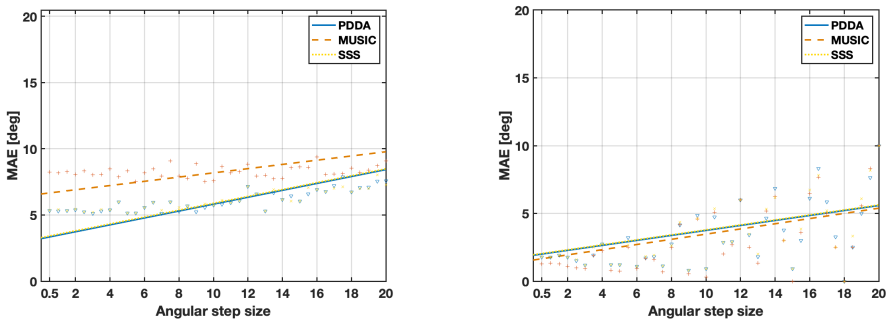

(a) Azimuth **(b)** Elevation

Figure 3.50: 12 elements square shaped for different angle step size

Observing the figures, we can identify that increasing the angular step results in a higher MAE. However, a bigger angular step-size shortens the computation time. Thus, in this trade off, a slightly bigger step-size can be used and still have a low MAE. We consider 5° of step-size sufficiently large to have a small error and an improved computation time.

3.4.6 Summary

We have analysed the performance of the DOA algorithms in terms of error accuracy, resolution, noise robustness, number of antenna elements used, number of BLE packets and snapshots used, and angular step-size. A summary of this comparison is shown in Table 3.11. We also add the computational complexity parameters such as, the covariance matrix computation, eigenvalue decomposition and the elapsed time given by MATLAB.

		PDDA	**MUSIC**	**SSS**	**ESPRIT**
Knowledge of the number of arriving signals		No	Yes	Yes	Yes
Covariance matrix		No	Yes	Yes	Yes
Eigenvalue decomposition		No	Yes	Yes	Yes
Angular search		Yes	Yes	Yes	No
MAE (°) 2x8 URA	Azimuth	4.72	4.90	4.69	10.81
	Elevation	12.33	12.69	12.33	11.24
MAE (°) 4x4 URA	Azimuth	4.15	6.84	4.66	12.51
	Elevation	4.21	4.39	4.12	4.31
MAE (°) 12 elements square shaped	Azimuth	5.30	8.21	5.33	11.89
	Elevation	1.78	1.33	1.75	3.62
Elapsed Time 198.000 iterations		22.5 ms	85.9 ms	35 ms	0.11 ms

Table 3.11: Summary of DOA algorithms performance

Definitive conclusions can be extracted from this table. First, we see how PDDA algorithm saves computation effort by not making use of the covariance function and the eigenvalue decomposition unlike MUSIC, SSS and ESPRIT. Moreover, it is not necessary to have knowledge about the number of sources in the system, which reduces its complexity further on. Regarding the measured MAE in the direction finding measurements, it can be seen that PDDA and SSS have very close results due to the mentioned equivalence between these algorithms, unlike MUSIC that gives slightly worse results. Finally, a 198.000 iteration simulation is been carried out in order to measure the average time that each DOA algorithm takes to compute their pseudo-spectrum. ESPRIT outperforms the rest of the algorithms because it is the only algorithm that do not perform an angular calculation of the pseudo-spectrum. However, the error accuracy penalizes ESPRIT, having approximately more than 6°of error in azimuth compared to the others. On the other hand, PDDA's elapsed time is 1.55 times faster than SSS and 3.81 times faster than MUSIC. Thus, we conclude that PDDA is the most compensated algorithm in terms of estimation accuracy and computational complexity. PDDA

is implemented in the last part of the thesis, the virtual positioning system. Together with PDDA we use the 4x4 URA since it is also a compensated array for angular estimation in both azimuth and elevation planes, presenting a MAE of only 4°.

Chapter 4

Positioning based on Bluetooth v5.1 Direction Finding

Once the analysis of Bluetooth v5.1 direction finding is done, it is time to use the knowledge and findings and apply them into a Bluetooth v5.1 position finding system. There are many ways of estimating the position of a tag and we have introduced the BLE technology with its latest version v5.1 as a very suitable technology to perform indoor positioning. We have given literature review about BLE indoor positioning. Specially, researchers from the University of Edinburgh concluded that sub-meter error accuracy is possible using Bluetooth v5.1 in indoor positioning. However their conclusions were based on SDR simulations. Thus, our aim in this final part of the thesis is to demonstrate that sub-meter error accuracy is possible using actual BLE v5.1 hardware in indoor positioning.

4.1 Measurement Scenario

To do so, we propose a new indoor scenario where the position finding measurements are carried out. The place is an office room with a high human mobility and large amount of possible scatters such as, tables, columns, walls and lamps. Figure 4.1 depicts an overview of the scenario looked from the floor plan.

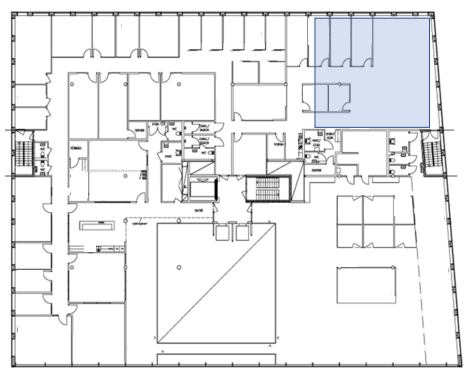

Figure 4.1: Position finding measurement scenario

To perform a position finding measurements, more than one receivers needs to be used in order to apply position estimation algorithms. As we showed on previous sections, direction finding is carried out with only one receiver. However, in order to estimate the position we need more than one estimated direction to apply geometric algorithms when estimating the position. We propose a four anchors or receivers positioning system. We use four in order to cover the area where the measurements are carried out. Figure 4.2 shows the scenario where the measurements took place together with the receiver and transmitter positions.

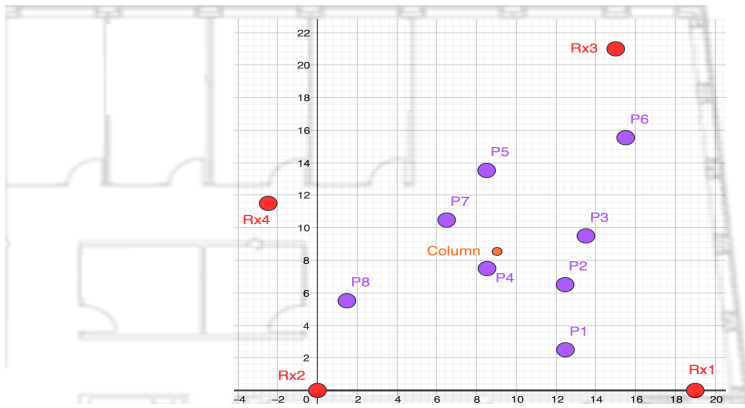

Figure 4.2: Position finding measurement scenario

Due to constraints in hardware equipment we can not use four different antenna arrays at the same time. We are using only the 4x4 URA and changing its position to Rx_1, Rx_2, Rx_3 and Rx_4 position as it is shown in Figure 4.2. From the transmitter perspective, we used eight different positions in the office room, from *P1* to *P8* position and the transmitter is the same used in the direction finding measurements. Thus, in total 32 different measurements are taken and the position finding measurement is emulated virtually. In figure 4.3 we show how the receiver is placed at the four positions. The 4x4 URA is placed at 2 m height in the four positions and the transmitter has 1.1 m height in all eight positions. The measurement procedure is the same as in the direction finding measurements with the exception that the receivers' orientation is fixed. Regarding the orientation of the array at the four receiving positions, a common reference has been selected. The 4x4 URA will be oriented towards the column at all receiving positions. That orientation allows the URA to gather energy around the direction of maximum gain and we avoid receiving directions from the edges of the array.

(a) Rx1 position

(b) Rx2 position

(c) Rx3 position

(d) Rx4 position

Figure 4.3: 4x4 URA at four receiving positions

4.2 Proposed Position Estimation Algorithm

Before exposing the results, in this section, we explain the procedure of estimating the position. We will rely on AOA and RSSI in order to estimate the position of the transmitter. Thus, it is a hybrid AOA-RSSI position estimation algorithm. The position parameter is given in a 2 dimensional coordinates system. So, a geometric space of the scenario should be built. As it can be seen from Figure 4.2, there are two axes and the origin is located at the Rx_2 position. This coordinates system will be used as the global coordinates system which represent the actual position of the transmitter. The scale of it is twice the real scale in meters. The following figure shows a representation of this geometric space.

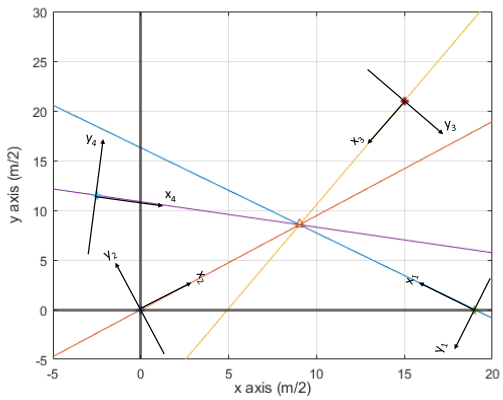

Figure 4.4: Geometric space of the scenario

In the geometric space there are four local axis that corresponds to the four receiving positions. The x axis of the local coordinates system is located perpendicularly to the 4x4 URA and pointing to the reference point. That direction corresponds to $\phi = 0°$, same as the coordinates used for direction finding measurements. The coloured lines represent the line function that intersects the receivers position and the reference point. These line functions will be tilted according to the estimated angle of arrival at each position. The estimated distance using the RSSI value will constrain the lines and it will result in four points. We propose to derive the geometric centrum of the points in order to obtain the estimated position. The geometric centrum for this system is defined as,

$$\hat{x} = \frac{1}{4}\sum_{i=1}^{4} \hat{x_i} \tag{4.1}$$

$$\hat{y} = \frac{1}{4}\sum_{i=1}^{4} \hat{y_i} \tag{4.2}$$

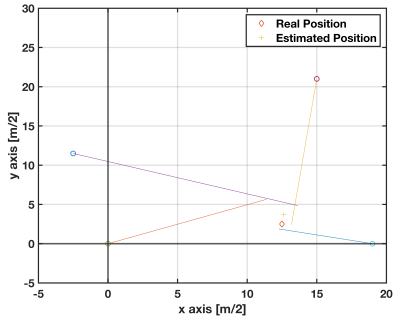

Figure 4.5: Geometric space of the scenario

Figure 4.5 shows an example of the utilisation of the AOA and the estimated distance given by the RSSI values. The length of each line represent the distance while the angle of each line respect to the reference point is the estimated direction from each receiver. This results in four points, and the estimated position is given by the geometric center of those points.

4.2.1 Path Loss Model

As we presented in the limitations section, further work should be done in order to come up with an accurate path loss model of this specific indoor environment. Measurements were carried out to build a model. However the accuracy of it has shown irregularities and inconsistencies. Thus, in order to add the RSSI parameter to the positioning estimation algorithm, further work and data analysis should be done and due to time constraints we are assuming knowledge of the distance between the transmitter and the receiver at each measurement point.

4.3 Results and Discussion

The parameters used in the position finding measurements are shown in Table 4.1.

Post-Processing Parameters	
Algorithm	PDDA
Arrays' orientation	zy plane
Spectrum's step size	$1°$
Azimuth range	$-90° \leq \theta \leq 90°$
Elevation range	$0° \leq \phi \leq 180°$
Number of BLE packets	48
Number of snapshots	16

Table 4.1: Post-processing parameters

In this position finding measurements, the computational effort is not an aspect to be analysed. The objective is to achieve sub-meter error accuracy using 48 BLE packets for each of the eight positions. In total 16 positions are estimated on each transmitting position. Once the position finding measurements are completed it is time to implement and take advantage of the previous direction finding measurements to use in signal processing. The proposed algorithm which makes use of frequency diversity to make the angular error accuracy more robust is used together with PDDA algorithm. After post-processing the data, the results are exposed in Table 4.2.

	Average Δm
Position 1	0.6198 m
Position 2	0.5819 m
Position 3	0.9178 m
Position 4	0.7612 m
Position 5	0.7465 m
Position 6	1.64 m
Position 7	0.2825m
Position 8	1.5516 m
Total average Δm	**0.8877 m**

Table 4.2: Average distance error

Δm represents the euclidean distance between the estimated position and the real position. The values in Table 4.2 corresponds to the average distance error of 16 estimations for each position. The total average distance error is 0.8877 m which is below the 1 m accuracy objective. Thus, we can conclude that the proposed positioning system provides sub-meter accuracy with Bluetooth v5.1 hardware. Figure 4.6 depicts the distribution of the estimated positions at each transmitting position. The distribution of the estimations is less confined in positions five, seven and eight. This is due to AOA estimation fluctuation given by the physical environment that impacts the electromagnetic wave propagation paths.

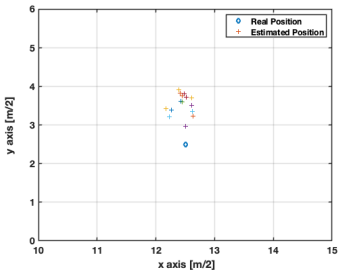

(a) Position 1

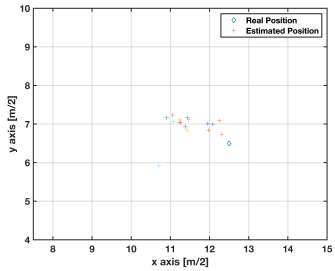

(b) Position 2

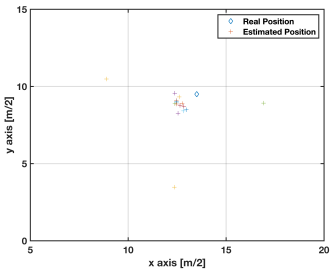

(c) Position 3

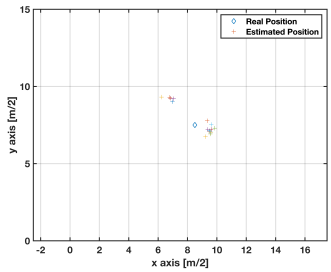

(d) Position 4

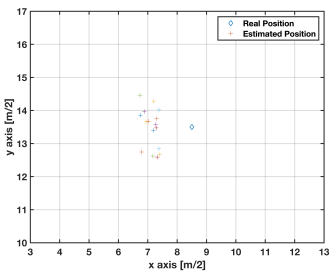

(e) Position 5

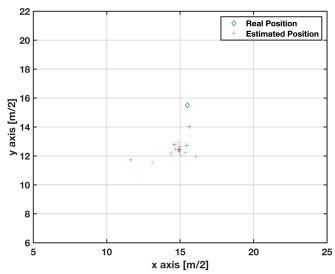

(f) Position 6

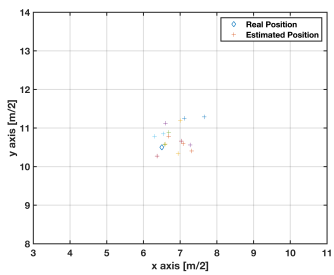

(g) Position 7

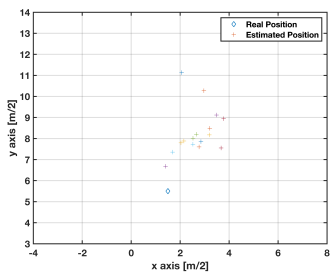

(h) Position 8

Figure 4.6: Positioning estimation results

Chapter 5
Conclusions

In this thesis we provide the reasons why the latest version of Bluetooth, the Bluetooth v5.1 enhances the positioning capabilities due to its new addition, the CTE, in the protocol. We demonstrated the benefit of its new feature by proposing a direction finding system in indoor environment. In this system we carried out a deep analysis of different DOA estimation algorithms and their performance in terms of angular estimation accuracy and computation complexity. Furthermore, different receiving antenna arrays are evaluated since as introduced in the theoretical background, the angular resolution depends on the characteristics of the receiving antenna array. In the process, we investigated the results of transmitting at the BLE advertising channels and see how the angular estimations are affected. We came up with an algorithm that makes the angular estimation error more robust thanks to frequency diversity. The analysis of DOA estimation algorithm provided us clear conclusions on which of the algorithms is more compensated in terms of angular estimation performance and computation complexity. PDDA results to be a promising algorithm that performs in a satisfactory manner together with the frequency diversity proposed algorithm. We comply successfully with the original 10°error threshold for the system reaching a MAE around 4°using a large set of data. Using the findings of direction finding measurements and post-processing we proposed a position finding system in order to test the algorithms used previously to determine the position of the transmitter. We implemented a simple positioning algorithm using both the AOA and RSSI parameters. Due to time constraints, the path loss model given by the RSSI values is assumed to be known and so the actual distance between the transmitter and the receiver is known. The results show us that sub-meter accuracy is possible using Bluetooth v5.1 hardware which complies with our positioning accuracy objective. All in all, we made a trip from theory to measurements and we have shown an enhanced positioning system using Bluetooth v5.1 .

5.1 Future work

There are very interesting research lines to be followed in the indoor positioning field. Regarding DOA estimation algorithms, we have used the first approach that was published for ESPRIT. However, ESPRIT algorithm evolved into unitary ESPRIT with the aim to reduce computational complexity using only the real numbers of the received data. This evaluation could make a difference comparing different DOA estimation algorithms. On the other hand, machine learning is a hot topic these years. It has shown promising results in many areas and it could also make a difference in positioning.

References

[1] F. Zafari, A. Gkelias and K. K. Leung, "A Survey of Indoor Localization Systems and Technologies," in IEEE Communications Surveys & Tutorials, vol. 21, no. 3, pp. 2568-2599, thirdquarter 2019, doi: 10.1109/COMST.2019.2911558.

[2] Hofmann-Wellenhof, B. and Lichtenegger, H. (2001) Global positioning system : theory and practice. 5., ed. Springer. Available at: https://search-ebscohost-com.ludwig.lub.lu.se/login.aspx?direct=true&db=cat07147a&AN=lub.1269948&site=eds-live&scope=site (Accessed: 13 May 2020)

[3] He, Z. et al. (2017) 'Evaluation of GPS/BDS indoor positioning performance and enhancement', Advances in Space Research, 59(3), pp. 870–876. doi: 10.1016/j.asr.2016.09.009.

[4] Cominelli, M, Patras, P & Gringoli, F 2019, Dead on Arrival: An Empirical Study of The Bluetooth 5.1 Positioning System.

[5] Cisco Meraki. Real-Time Location Services (RTLS).

[6] Apple Developer.https://developer.apple.com/ibeacon/.(Accessed: 13 May 2020)

[7] xnp.https://www.nxp.com/docs/en/brochure/75016740.pdf(Accessed: 13 May 2020)

[8] Medium. 2020. Bluetooth Technology: What Has Changed Over The Years. [online] Available at: <https://medium.com/jaycon-systems/bluetooth-technology-what-has-changed-over-the-years-385da7ec7154> (Accessed 14 May 2020).

[9] Bluetooth® Technology Website. 2020. Bluetooth Technology Website | The Official Website Of Bluetooth Technology.. [online] Available at: <https://www.bluetooth.com/> (Accessed 14 May 2020).

[10] T. V. Haute et al., "Platform for benchmarking of RF-based indoor localization solutions," in IEEE Communications Magazine, vol. 53, no. 9, pp. 126-133, September 2015, doi: 10.1109/MCOM.2015.7263356.

[11] Bluetooth Technology Website. (2020). Bluetooth Direction Finding: A Technical Overview | Bluetooth Technology Website. [online] Available at: https://www.bluetooth.com/bluetooth-resources/bluetooth-direction-finding/(Accessed 27 Feb. 2020).

[12] Paulraj, A., Nabar, R. and Gore, D., 2008. Introduction To Space-Time Wireless Communications. Cambridge: Cambridge University Press.

[13] Bluetooth Technology Website. (2020). Bluetooth Core Specification v5.1:Feature Overview. [online] Available at: https://www.bluetooth.com/events/launch-preview-bluetooth-core-specification-v5-1/ (Accessed 14 May 2020)

[14] F. Zafari, I. Papapanagiotou and K. Christidis, "Microlocation for Internet-of-Things-Equipped Smart Buildings," in IEEE Internet of Things Journal, vol. 3, no. 1, pp. 96-112, Feb. 2016, doi: 10.1109/JIOT.2015.2442956

[15] Bluetooth Technology Website. (2020). Bluetooth 5.0 : Go Faster. Go Further. [online] Available at: https://www.bluetooth.com/wp-content/uploads/2019/03/Bluetooth_5-FINAL.pdf

[16] K. Witrisal et al., "High-Accuracy Localization for Assisted Living: 5G systems will turn multipath channels from foe to friend," in IEEE Signal Processing Magazine, vol. 33, no. 2, pp. 59-70, March 2016, doi: 10.1109/MSP.2015.2504328.

[17] Z. M. Jawad Kubba and H. K. Hoomod, "The Internet of Everything Based Smart Systems: Applications and Challenges," 2019 1st AL-Noor International Conference for Science and Technology (NICST), Sulimanyiah - Kurdistan Region- IRAQ, Iraq, 2019, pp. 58-62, doi: 10.1109/NICST49484.2019.9043785.

[18] SIG Bluetooth. Specification of the bluetooth system covered-core package version: 4.0, 2010.

[19] Bluetooth Technology Website. (2020). An Introduction to Bluetooth Beacons. [online] Available at: https://www.bluetooth.com/bluetooth-resources/beacon-smart-starter-kit/

[20] S. Monfared, T. Nguyen, L. Petrillo, P. De Doncker and F. Horlin, "Experimental Demonstration of BLE Transmitter Positioning Based on AOA Estimation," 2018 IEEE 29th Annual International Symposium on Personal, Indoor and Mobile Radio Communications (PIMRC), Bologna, 2018, pp. 856-859, doi: 10.1109/PIMRC.2018.8580796.

[21] Molisch., 2011. Wireless Communications, Second Edition. Wiley-IEEE Press.

[22] Al-Sadoon, M., Ali, N., Dama, Y., Zuid, A., Jones, S., Abd-Alhameed, R. and Noras, J. (2017). A New Low Complexity Angle of Arrival Algorithm for 1D and 2D Direction Estimation in MIMO Smart Antenna Systems. Sensors, 17(11), p.2631.

[23] Madisetti, V. and Madisetti, V., 2010. Wireless, Networking, Radar, Sensor Array Processing, And Nonlinear Signal Processing. Hoboken: Taylor and Francis.

[24] X. Li, D. Xu, X. Wang and R. Muhammad, "Design and implementation of indoor positioning system based on iBeacon," 2016 International Conference on Audio, Language and Image Processing (ICALIP), Shanghai, 2016, pp. 126-130, doi: 10.1109/ICALIP.2016.7846648.

[25] X. Lin, T. Ho, C. Fang, Z. Yen, B. Yang and F. Lai, "A mobile indoor positioning system based on iBeacon technology," 2015 37th Annual International Conference of the IEEE Engineering in Medicine and Biology Society (EMBC), Milan, 2015, pp. 4970-4973, doi: 10.1109/EMBC.2015.7319507.

[26] J. Powar, C. Gao and R. Harle, "Assessing the impact of multi-channel BLE beacons on fingerprint-based positioning," 2017 International Conference on Indoor Positioning and Indoor Navigation (IPIN), Sapporo, 2017, pp. 1-8, doi: 10.1109/IPIN.2017.8115871.

[27] Randolph, J., 1969. Calculus And Analytic Geometry. Belmont, Calif.: Wadsworth Pub Co.

[28] Chen, Z., Gokeda, G. and Yu, Y., 2010. Introduction To Direction-Of-Arrival Estimation. Boston: Artech House.

[29] R. Schmidt, "Multiple emitter location and signal parameter estimation," in IEEE Transactions on Antennas and Propagation, vol. 34, no. 3, pp. 276-280, March 1986, doi: 10.1109/TAP.1986.1143830.

[30] A. Zhao, H. Jiang and S. Li, "Improved capon estimators for DOD and DOA estimation in large array MIMO radar: A random matrix method," 2018 IEEE Radar Conference (RadarConf18), Oklahoma City, OK, 2018, pp. 1140-1145, doi: 10.1109/RADAR.2018.8378722.

[31] H. Krim and M. Viberg, "Two decades of array signal processing research: the parametric approach," in IEEE Signal Processing Magazine, vol. 13, no. 4, pp. 67-94, July 1996, doi: 10.1109/79.526899.

[32] Al-Sadoon MAG, Ali NT, Dama Y, Zuid A, Jones SMR, Abd-Alhameed RA, Noras JM. A New Low Complexity Angle of Arrival Algorithm for 1D and 2D Direction Estimation in MIMO Smart Antenna Systems. Sensors (Basel). 2017 Nov 15;17(11):2631. doi: 10.3390/s17112631. PMID: 29140313; PMCID: PMC5713173.

[33] Al-Sadoon, Mohammed & Abduljabbar, Nabeel & Ali, Nazar & Asif, R. & Zweid, A. & Alhassan, Hanifatu & Noras, J.M. & Abd-Alhameed, Raed. (2019). A More Efficient AOA Method for 2D and 3D Direction Estimation with Arbitrary Antenna Array Geometry: 9th International EAI Conference, Broadnets 2018, Faro, Portugal, September 19–20, 2018, Proceedings. 10.1007/978-3-030-05195-2_41.

[34] N. Karmous, M. O. El Hassan and F. Choubeni, "An Improved Esprit Algorithm for DOA Estimation of Coherent Signals," 2018 International Conference on Smart Communications and Networking (SmartNets), Yasmine Hammamet, Tunisia, 2018, pp. 1-4, doi: 10.1109/SMARTNETS.2018.8707432.

[35] H. Tataria, P. J. Smith and P. A. Dmochowski, "On the General Analysis of Coordinated Regularized Zero-Forcing Precoding: An Application to Two-Tier Small-Cell Networks," in IEEE Transactions on Communications, vol. 65, no. 7, pp. 3133-3150, July 2017, doi: 10.1109/TCOMM.2017.2695199.

[36] Bluetooth Technology Website. (2020). Enhancing Bluetooth Location Services with Direction Finding. [online] Available at: https://www.bluetooth.com/bluetooth-resources/enhancing-bluetooth-location-services-with-direction-finding/

[37] C. S. Mouhammad, A. Allam, M. Abdel-Raouf, E. Shenouda and M. Elsabrouty, "BLE Indoor Localization based on Improved RSSI and Trilateration," 2019 7th International Japan-Africa Conference on Electronics, Communications, and Computations, (JAC-ECC), Alexandria, Egypt, 2019, pp. 17-21, doi: 10.1109/JAC-ECC48896.2019.9051304.

[38] Hjelle, O., Dæhlen, M. and NetLibrary, I. (2006) Triangulations and applications. [Elektronisk resurs]. Springer (Mathematics and visualization). Available at: https://search.ebscohost.com/login.aspx?direct=true&db=cat07147a&AN=lub.5709641&site=eds-live&scope=site(Accessed: 20May2020).

[39] U-blox.com. 2020. [online] Available at:<https://www.u-blox.com/en/docs/UBX-19049405> [Accessed 21 May 2020].

[40] U-blox.com. 2020. [online] Available at: <https://www.u-blox.com/en/docs/UBX-17056481> [Accessed 21 May 2020].

[41] Roy, R. and Kailath, T., 1989. ESPRIT-estimation of signal parameters via rotational invariance techniques. IEEE Transactions on Acoustics, Speech, and Signal Processing, 37(7), pp.984-995.

[42] Bluetooth.org. 2020. [online] Available at: <https://www.bluetooth.org/docman/handlers/downloaddoc.ashx?doc_id=457080> [Accessed 23 May 2020].

[43] Hoffman, C. and Driggers, R., 2015. Encyclopedia Of Optical And Photonic Engineering. Boca Raton: CRC.

[44] Ericsson. 2020. [online] Available at: https://www.ericsson.com/49d1d9/assets/local/mobility-report/documents/2019/ericsson-mobility-report-june-2019.pdf